LA-10557-PR
Progress Report

Los Alamos National Laboratory is operated by the University of California for the United States Department of Energy under contract W-7405-ENG-36.

Space Nuclear Safety Program

June 1984

Los Alamos
Los Alamos National Laboratory
Los Alamos, New Mexico 87545

DISCLAIMER

The four most recent reports in this series, unclassified, are LA-10190-PR, LA-10511-PR, LA-10526-PR, and LA-10536-PR.

This work was supported by the US Department of Energy, Office of Special Nuclear Projects.

Edited by Renate Lewin
Photocomposition by Joyce A. Martinez

LA-10557-PR
Progress Report

UC-33A
Issued: November 1985

LA--10557-PR

DE86 007197

Space Nuclear Safety Program

June 1984

Compiled by
T. G. George

Los Alamos National Laboratory
Los Alamos, New Mexico 87545

SPACE NUCLEAR SAFETY PROGRAM

June 1984

Compiled by
T. G. George

ABSTRACT

This technical monthly report covers studies related to the use of $^{238}PuO_2$ in radioisotope power systems carried out for the Office of Special Nuclear Projects of the US Department of Energy by Los Alamos National Laboratory. Most of the studies discussed are ongoing; the results and conclusions described may change as the work continues.

I. GENERAL-PURPOSE HEAT SOURCE (GPHS)/SAFETY VERIFICATION TEST (SVT) SERIES

A. SVT-6 Postmortem Examination (T. George)

Details of the test conditions, module disassembly, and initial metallography were given in previous monthly reports. In this month we completed metallographic examination of the clads and plutonia fuel, and received the results of Auger and spectrographic analyses.

1. Vent Metallography. Metallographic examination of the vents on capsules HF-361 and HF-373 did not reveal any mechanical defects (Figs. 1 and 2). Both frits were uniform and properly aligned. No large inclusions or glassy oxides were observed in either vent.

Wall sections adjacent to both vents exhibited an unusual amount of grain coarsening (Figs. 3 and 4). Areas adjacent to the HF-373 vent contained as few as 2 grains/thickness; in one section a nearly continuous grain boundary extended from the interior to the surface (Fig. 4). Although excessive grain growth in both vent sections occurred next to the cover welds, the microstructures did not appear to have resulted from welding.

Further examination of the vent sections revealed deep cracks on the radius of each vent cup, 180° to the impact face (Figs. 5 and 6). The cracks in both cups initiated on the interior surface and occurred in regions of moderate grain growth. Although exact lengths could not be determined, the cracks in HF-361 appeared to penetrate more than 50% of the capsule wall. The cracks in HF-373 traversed more than 65% of the wall thickness.

2. Fuel Ceramography. Ceramographic examination of specimens removed from the HF-361 and HF-373 fuel pellets did not reveal any unusual features. Both fuel samples had a typical microstructure (Figs. 7 and 8).

3. Chemical Analyses. Specimens for spectrographic analysis were removed from each of the prime clads. Two additional samples for Auger electron spectroscopy (AES) were also obtained from each cup. Results of the spectrographic analyses are given in Table I; the AES results are listed in Tables II and III.

Results of the spectrographic analyses indicate that all of the iridium cups had similar chemistries; cup-to-cup variations were not significant. The Auger results suggest that all of the interior cup surfaces were thorium depleted. Thorium content on the interior of the HF-373 vent cup was extremely low. Electron images of

TABLE I. Spectrographic Analyses of SVT-6 Primary Clads (ppm)

	HF-361		HF-373	
Element[a]	Vent Cup	Blind Cup	Vent Cup	Blind Cup
Fe	150	200	200	200
Al	60	50	50	50
Ca	<3	<3	<3	3
Ni	40	30	40	40
Si	10	<10	<10	30
Cr	30	15	40	30
Cu	15	5	3	3
Pt	30	<30	<30	<30
Ru	<30	30	<30	<30
W	0.1-1.0%	0.1-1.0%	0.1-1.0%	0.1-1.0%

[a]Elements are listed only if they exceed detectability limits in at least one sample.

TABLE II. AES Results for Sections Removed from Capsule HF-361

	Th_{65}/Ir_{229}	C_{270}/Ir_{229}	O_{510}/Ir_{229}	S_{150}/Ir_{229}	Cl_{180}/Ir_{229}
Vent cup					
Adjacent to fracture					
inside	0.326	0.140	0.628	—	—
center	0.516	0.036	0.309	—	—
outside	0.629	0.112	0.629	—	—
180° from fracture					
inside	0.194	0.097	0.726	0.097	—
center	0.440	0.120	1.100	—	—
outside	0.533	0.100	1.125	0.167	—
Weld-shield cup					
Adjacent to fracture					
inside	0.379	0.035	0.690	—	—
center	0.490	0.061	0.449	—	—
outside	0.556	0.167	0.907	—	—
180° from fracture					
inside	0.140	1.590	0.947	strong[a]	0.193
center	0.417	0.083	0.917	—	—
outside	0.305	0.678	0.712	0.169	0.136

[a]Results indicated a strong sulfur line that overlapped onto adjacent peaks.

TABLE III. AES Results for Sections Removed from Capsule HF-373

	Th_{65}/Ir_{229}	C_{270}/Ir_{229}	O_{510}/Ir_{229}	S_{150}/Ir_{229}	Cl_{180}/Ir_{229}
Vent cup					
Impact face					
inside	**0.068**	**0.091**	**0.386**	—	—
center	**0.778**	**0.028**	**0.556**	—	—
outside	**0.541**	**0.432**	**0.730**	—	—
180° from impact face					
inside	**0.023**	**0.140**	**0.512**	—	—
center	**0.542**	**0.083**	**0.583**	—	—
outside	**0.578**	**0.133**	**0.622**	—	—
Weld-shield cup					
Impact face					
inside	**0.154**	**0.135**	**0.538**	—	—
center	**0.640**	**0.100**	**0.680**	—	—
outside	**0.364**	**0.455**	**0.682**	—	—
180° from impact face					
inside	**0.400**	**1.870**	**0.545**	**0.109**	—
center	**0.417**	**0.896**	**0.667**	—	—
outside	**0.400**	**1.000**	**0.600**	—	—

the thorium-depleted cup sections did not reveal abnormal grain growth.

Samples for chemical analysis were removed from each of the SVT-6 fuel pellets. Results of spectrographic analyses are listed in Table IV. Significant differences in chemistry were not apparent. The SVT-6 fuel pellets were similar to one another and to fuel pellets used in previous SVT tests.

4. Particle Size Analyses. To quantify the impact response of the fuel, we selected capsule HF-361 (unbreached) for a particle size analysis. The capsule was opened underwater (to prevent the loss of small fuel fragments) and defueled. The fuel fragments were sized by passing them through a series of screens. Results of the particle size analysis are given in Tables V and VI.

As part of the ongoing effort to determine the amount and size of fines released by a breached clad, the graphite impact shells (GISs) and the aeroshell used in SVT-6 were ultrasonically cleaned and burned, and the remains were analyzed for plutonium. The results are listed in Table VII. The ultrasonic cleaning solution and finely divided catch-tube debris were dried and placed in a low-temperature ashing furnace, and the remains were sized and analyzed for plutonium. These results are given in Table VIII. We combined the plutonium content of the SVT-6 graphitics with the plutonium contained in the catch tube to give a total release figure of 0.0149 g.

B. SVT-7 Postmortem Examination (D. Pavone)

This test assembly was aged 90 days at 1287°C, subjected to a 1375°C pulse to simulate orbital-decay reentry temperature, and impacted in the $\alpha = 15°$, $\beta = 0°$, $\gamma = 0°$ orientation against a steel target at 975°C and 53.5 m/s. The test components are listed in Table IX.

Figure 9 illustrates the condition of the module as recovered from the catch tube. The aeroshell fractured along the axial contact lines of the leading GIS, and a partial fracture on the impact face occurred parallel to the axis of the trailing GIS. A dent, with associated fractures, was also present on the back side of the aeroshell. Damage to both impact shells was similar, with irregular cracks on the impact face traversing about 80% of the length and a transverse crack on the back side near the closure (Figs. 10 and 11). Damage to the secondary GIS was most severe; the cap was ejected and a piece of the impact-shell back was torn from the body.

TABLE IV. Spectrographic Analyses of the SVT-6 Fuel Pellets (ppm)

Elements[a]	HF-189	HF-225	HF-361	HF-373
Ag	2	1	20	15
Fe	20	15	10	20
Mg	3	10	20	4
Al	65	45	30	15
Ti	20	10	20	20
Na	8	10	<2	15
Si	25	30	35	45
Ca	<3	60	150	130
Cu	<1	<1	<1	8
Mn	<1	<1	4	<1
Cr	<5	<5	15	<5

[a]Elements are listed only if they exceed detectability limits in at least one sample.

TABLE V. Sieve Analysis of the Fuel in Capsule HF-361

Particle Size (μm)	Weight Fraction	Accumulated Weight Fraction
+6000	0.0464	0.0464
+2000	0.1901	0.2365
+ 841	0.3146	0.5511
+ 420	0.2193	0.7704
+ 177	0.1296	0.9000
+ 125	0.0212	0.9212
+ 74	0.0242	0.9454
+ 44	0.0174	0.9628
+ 30	0.0104	0.9732
+ 20	0.0122	0.9854
+ 10	0.0048	0.9902
− 10	0.0098	1.0000

TABLE VI. Subsieve Particle Distribution of Fuel in Capsule HF-361

Particle Size Range (μm)	Weight Fraction	Accumulated Weight Fraction
0 to 1	0.000846	0.000846
1 to 2	0.000492	0.001338
2 to 3	0.000635	0.001973
3 to 4	0.000800	0.002773
4 to 5	0.001000	0.003773
5 to 6	0.000972	0.004746
6 to 7	0.000172	0.004917
7 to 8	0.000768	0.005685
8 to 9	0.001094	0.006779
9 to 10	0.003001	0.009780

TABLE VII. Plutonium Content of the SVT-6 Graphitics

Components	Pu Content (g)
GIS A (PGT-1023)	0.0085
GIS C (PGT-1026)	0.0001
Aeroshell (PAT-1009)	0.0002

TABLE VIII. Size and Quantity of Plutonium Released into SVT-6 Catch Tube[a]

Particle Size (μm)	Weight (g)
0 – 10	0.0003
10 – 20	0.0010
20 – 420	0.0048

[a]Included are particles recovered from the aeroshell and GIS ultrasonic cleaning solution.

TABLE IX. SVT-7 Components

Component	Number
Aeroshell	PAT-1010
Prime impact assembly	
Impact shell	PGT-1020
Fueled clads	FC-364 and FC 368
Fuel pellets	HF-364 and HF-368
Insulation sleeve	C-40-9
Insulation disks	P-11-1-32, P-12-1-4
Secondary impact assembly	
Impact shell	PGT-1021
Fueled clads	FC-165 and FC-112
Fuel pellets	HF-165 and HF-112
Insulation sleeve	C-38-3
Insulation disks	P-12-1-3, P-11-2-34

The impacted fueled clads are shown in Figs. 12 and 13. Major failures attributable to fuel-fragment push-through occurred on the FC-364 (primary clad) impact face and on the back side of FC-165 (secondary clad). On FC-165, a fracture about 1 cm long × 0.5 cm wide occurred along the weld-bead centerline near the impact face. Minor fractures were present on the vent cup side of the FC-112 weld bead and on the vent cup radius of the FC-368 trailing face. Table X lists the gross deformation of the fueled clads and the estimated fracture areas. The clad deformations were similar to those observed in assemblies impacted in the $\alpha = 0°$ orientation.

Fracture patterns of the plutonia pellets are shown in Fig. 14. The fracture pattern of pellet HF-368 consisted of small, radially oriented columnar fragments. In contrast, the fracture patterns of pellets HF-364, HF-165, and HF-112 showed relatively large, randomly oriented fragments.

A fracture on the FC-368 vent cup radius is shown in Fig. 15. Visual examination of the interior surface did not indicate any penetration of the capsule wall, although metallographic examination indicated that the fracture had penetrated 50% of the wall thickness. Though the fracture mode was intergranular, a small reduction of thickness at the side of the fracture, about 2%, indicated limited ductility.

Figure 16 shows the interior of the failures on the back side of FC-112. The failures occurred in the vent-cup side of the weld bead, just beyond the tip of the weld overlap "spear point." The vent cup failure sites are

TABLE X. Impact Test Summary, GPHS SVT Series

Test No.	Rentry Mode	Clad No.	NDT[a] Value	Gross Deformation			Failures	
				Diam (%)	Height (%)	Axial (%)	Number	Area (mm)^2
SVT-1	Min-γ[b],	FC-232	3.0	+13.5	−11.1	+5.8	0	25.4
	Face-on	FC-238	5.0	+ 9.6	− 7.3	+3.8	0	
		FC-261	8.7	+11.7	−11.1	+5.6	2	
		FC-410	12.6	+ 9.8	− 9.6	+1.4	1	
SVT-2	Min-γ[b],	FC-355	6.8	+10.0	−10.4	+4.1	0	8.4
	Face-on	FC-369	6.0	+ 9.1	− 9.3	+4.1	0	
		FC-449	13.7	+12.5	−10.3	+5.6	3	
		FC-273	10.7	+10.3	−10.5	+4.4	0	
SVT-3	Orbital	FC-343	2.9	+12.3	− 9.0	+5.7	0	
	decay[c],	FC-350	1.1	+10.0	− 8.5	+2.6	0	
	Face-on	FC-457	9.8	+10.8	− 7.2	+5.6	0	
		FC-454	12.8	+ 9.5	− 6.4	+2.9	1	
SVT-4	Orbital	FC-348	1.0	+11.5	−11.3	+6.4	1	1.8
	decay,	FC-354	3.2	− 8.5	+ 8.2	+4.0	0	
	Face-on	FC-449	13.7	+12.5	− 8.5	+5.1	0	
		FC-273	10.7	+10.3	− 9.3	+3.4	0	
SVT-5	Orbital	FC-267	3.0	+10.4	− 9.1	+5.5	0	
	decay,	FC-260	4.0	+10.9	−13.7	+4.1	0	
	Side-on	FC-515	9.4	+ 5.5	− 4.5	+1.2	0	
		FC-426	9.6	+ 5.0	− 6.9	nil	0	
SVT-6	Orbital	FC-373	4.1	+11.2	−14.9	+ 6.2	2	24.1
	decay,	FC-361	4.4	+12.3	−17.6	+ 8.8	0	
	Side-on	FC-225	13.2	+ 7.8	− 8.8	+ 3.7	0	
		FC-189	13.3	+ 6.4	− 7.2	+ 2.9	0	
SVT-7	Orbital	FC-364	2.0	+ 9.9	−13.5	+ 5.3	1	53.0
	decay,	FC-368	1.6	+ 9.5	− 9.9	+ 5.4	0	
	α=15°	FC-165	13.0	+10.7	−10.0	+ 5.7	2	
		FC-112	11.0	+ 8.0	− 9.5	+ 4.0	2	

[a]Nondestructive testing.
[b]Aged 200 h at 1287°C (clad); impact at 919°C and 54 m/s.
[c]Aged 90 days at 1287°C (clad); impact at 975°C and 54 m/s.

shown in Fig. 17. One of the fractures exhibited a reduction in thickness of about 9%. The microstructure of the weld-bead was relatively large grained and nearly equiaxed at the fracture sites (Fig. 18). The fractures followed the grain boundaries across the weld bead thickness. It was not clear whether the fractures resulted solely from mechanical deformation, or from enlargement of preexisting cracks. The fact that the fractures occurred only on the vent cup side of the weld bead supports the latter.

C. SVT-8 Postmortem Examination (T. George)

A fully loaded GPHS module was impacted at 54.6 m/s and 975°C. The module orientation was $\alpha = 15°$, $\beta = 0°$, $\gamma = 0°$ (Fig. 19). Before impact, the test assembly was subjected to a simulated reentry temperature of 1375°C, and the fueled clads had been aged for 90 days at 1287°C. Encapsulation details for the SVT-8 clads are given in Table XI; data describing the fuel pellets are presented in Table XII. After the test, a sealed catch tube containing the impacted module was transferred to Wing 2 of the CMR building. Postmortem examination of the module began immediately.

The catch tube was placed in an open-fronted hood and the pump-out plug was removed. A swab inserted into the pump-out hole registered >20,000 counts/min/cm^2. The end of the catch tube was removed, and the inner nickel can (a radiation shield) was extracted with tongs. The impact assembly was then extracted and placed on a bed of solid CO_2. As in previous SVTs, even after extraction of the radiation shield and impact assembly, the catch tube contained a significant amount of debris (Fig. 20). The largest pieces of graphite were removed from the catch tube, and the remaining contents were washed and packaged for low-temperature ashing.

Aeroshell damage was significant (Fig. 21). Both closure caps were removed, and the aeroshell body was partially fractured along the axial contact lines of the leading GIS. Although both GISs were unrestrained, neither left the aeroshell.

Damage to the GISs was significant (Figs. 22 and 23) but not unusual. The caps on both GISs had been removed, and FC-437 (prime GIS) was released into the aeroshell.

The fuel capsules were extracted from the GISs, photographed, and measured. Side and end views of each capsules are shown in Fig. 24. Capsule dimensions and calculated gross strains are listed in Tables XIII and XIV.

Macroscopic examination revealed that the prime clads (FC-436 and FC-437) experienced only moderate

TABLE XI. Encapsulation Details for SVT-8 Fueled Clads

Capsule No.	SRP/NDT[a] Crack Indication	Iridium Cups		Fuel Pellet
		Vent	Weld Shield	
FC-391	9.8	RR925-3	RR920-5	8205HF391
FC-436	1.0	R919-4	R901-2	8207HF436
FC-437	1.0	MER41-1	MER41-2	8207HF437
FC-441	9.6	MER21-6	MER21-1	8207HF441

[a]Savannah River Plant nondestructive testing.

TABLE XII. Data for SVT-8 Fuel Pellets

Capsule No.	Fuel Form	Diameter (mm)	Length (mm)	Weight (g)	Fuel Pellet Process Atmosphere
FC-391	8205HF391	27.7	ni[a]	150.3	Argon
FC-436	8207HF436	27.7	27.7	150.1	Argon
FC-437	8207HF437	ni	ni	149.8	Argon
FC-441	8207HF441	27.6	27.9	150.6	Argon

[a]Nonintegral at loading.

TABLE XIII. Dimensions of the SVT-8 Fueled Clads

		FC-391	FC-436	FC-437	FC-441
Preimpact dimensions (mm)					
Diameter		29.77	29.77	29.79	29.77
Length		29.97	29.97	29.97	29.97
Postimpact dimensions (mm)					
Diameter					
Vent Cup	min	26.80	28.46	27.83	27.44
	max	32.40	31.34	32.47	32.03
Weld	min	26.86	28.82	27.42	27.85
	max	33.80	31.94	32.64	32.96
Blind Cup	min	26.71	27.42	27.07	26.79
	max	32.44	31.58	32.10	32.33
Length	min	31.18	30.48	30.45	31.14
	max	32.40	31.38	32.52	31.78

TABLE XIV. Postimpact Strains in the SVT-8 Fueled Clads

		FC-391	FC-436	FC-437	FC-441
Diameter					
Vent cup	min	− 9.98%	− 4.40%	− 6.58%	− 7.83%
	max	+ 8.83	+ 5.27	+ 9.00	+ 7.59
Weld	min	− 9.77	− 3.19	− 7.96	− 6.45
	max	+13.54	+ 7.29	+ 9.56	+10.71
Blind cup	min	−10.28	− 7.89	− 9.13	−10.00
	max	+ 8.97	+ 6.08	+ 7.75	+ 8.60
Length	min	+ 4.03	+ 1.70	+ 1.60	+ 3.90
	max	+ 8.10	+ 4.70	+ 8.51	+ 6.04

deformation. Although capsule FC-437 had been released from the GIS, it did not appear to be significantly more deformed than capsule FC-436, which remained in the GIS.

Examination of clads removed from the trailing GIS (FC-391 and FC-441) revealed that capsule FC-391 had breached. The closure weld on capsule FC-391 opened over a 120° arc (Fig. 25), with the crack center 90° to the impact face; the weld-shield band remained in place and limited fuel release. The crack was approximately 30.0 mm × 1.8 mm and had an area of 39.7 mm^2. The crack width permitted excessive clad deformation and generated secondary cracks in the vent and weld-shield cups (Fig. 26). Capsule FC-441 experienced moderate deformation and contained no visible defects.

An abrasive cutting wheel was used to make a narrow circumferential slit 8-10 mm above the weld (blind cup) on capsules FC-436, FC-441, and FC-391. The capsules were pried open with a small screw driver, and the patterns of fuel fracture were photographed (Fig. 27-29). The capsules were then defueled.

To determine the quantity of respirable fuel particles produced by the impact, we selected capsule FC-437 for a particle size analysis. The capsule was transferred to a

glove-box train used for fines analysis and was opened underwater to prevent the loss of small fuel fragments. The fuel breakup in FC-437 (Fig. 30) was similar to that observed in the other capsules.

II. LIGHT-WEIGHT RADIOISOTOPE HEATER UNIT (LWRHU) (C. Land)

A. Bullet Test

A LWRHU capsule (RS-3 or 18480) fueled with UO_2 was impacted with a .50-caliber, 18-g aluminum-alloy (2219/T87) bullet at 2979 ft/s (908 m/s). The capsule was set in an aluminum cup (see Fig. 31) held in position by an aluminum ring and was impacted 90° to the closure end (Fig. 32). The capsule deformed in the closure weld area but did not breach.

A longitudinal section of the fueled capsule showed that the fuel was crushed at the impacted end (Fig. 33). Both halves of the capsule were mounted and polished (Fig. 34); no vent hole was found. The closure weld was quite porous (Fig. 35), and the RS-3 vent-end weld was somewhat heavy but otherwise acceptable (Fig. 36). This was not a particularly severe test for this unit.

B. Fines Analysis

Fines analysis for the aged and impacted units (RHU-09-09 or 17870 and RHU-10-12 or 17869) are listed in Table XV. In the aged unit (RHU-09-09) that was impacted side-on, the total weight fractions of the <20-μm material (0.0576) was double that observed in RHU-09-02 (0.0252). The weight fraction of <20-μm material (0.016) in the aged unit was similar to the 0.013 weight fraction observed in RHU-09-03; both units were impacted 45° to the closure weld. Note that in the side-on impact (RHU-09-09), 60% of the material was approximately +420 μm, whereas in the corner-on impact (RHU-10-12), approximately 90% of the material was +420 μm. The distribution of the <10-μm size fraction (RHU-09-09) is listed in Table XVI.

TABLE XV. Fines Analysis

Particle Size (μm)	RHU-09-09 (wt. fraction)	RHU-10-12 (wt. fraction)
+420	0.5886	0.9147
+125	0.2435	0.0425
+ 20	0.1103	0.0268
+ 10	0.0183	0.0054
− 10	0.0393	0.0106

TABLE XVI. Subsieve Fines Analysis (<10 μm)

Particle Size (μm)	RHU-09-09 (wt. fraction)	RHU-10-12 (wt. fraction)
1	0.005	0.001
2	0.006	0.001
3	0.007	0.001
4	0.004	0.001
5	0.005	0.001
6	0.004	0.001
7	0.001	0.001
8	0.005	0.000
9	0.002	0.000
10	0.000	0.003

III. SAFETY TECHNOLOGY

A. Iridium Biaxial Testing (T. George)

Four iridium disks were impacted; numbers and test conditions are given in Table XVII. All four tests duplicated previous impacts and were designed to reinforce our data base. The results will be analyzed in the future.

Twelve 2.50-in. × 0.375-in. tensile specimens were returned from the machine shop and were immediately forwarded for photoresist gridding. If the tensile specimens are gridded soon, we will begin testing in August.

TABLE XVII. Summary of Biaxial Testing Completed in June 1984

Disk No.	Nominal Grains/Thickness	Test Temperature (°C)	Velocity (m/s)	Strain State
VR235-2	5.0	1440	45.00	+,0
Z563-5	25.0	1000	44.75	+,0
Z561-6	25.0	800	45.39	+,0
Z563-2	25.0	600	43.87	+,0

B. Iridium Chemistry (K. Axler)

The formation of P/Th/Ir compounds along DOP-26 iridium grain boundaries could adversely affect the impact behavior of iridium-encapsulated heat sources. In this month we continued with our investigation of P/Th/Ir ternary compounds. Thorium, iridium, and phosphorus were mixed in a molar proportion of 1:1:2 and pressed at 3000 psi. The pellet was sealed in an evacuated quartz tube and heated for 24 h at 1200°C. The products were Th_3P_4 (90%) and IrP_2 (10%). A sample of this mixture was placed in an evacuated tantalum cell and heated for 1 h at 1400°C; subsequent *x*-ray diffraction revealed the presence of a Th/Ir/P ternary.

C. Plutonium/Refractory Metal Compounds (R. Rhoe and K. Axler)

We prepared a sample of $PuRe_2$ by arc-melting the components and annealing them in an evacuated quartz ampule for 1 week. A fraction of the resulting intermetallic was placed in a tungsten effusion cell and the sublimation studied over the range 1500-2000°C. A $^{239}Pu^+$ species was observed and then analyzed with the mass spectrometer to determine the vapor pressure. The temperature dependence of the plutonium ion intensity yielded an 82.5-kcal heat of sublimation, which is that of elemental plutonium. This indicates that the sample decomposes when heated above 1500°C. We are taking additional measurements to determine the onset of decomposition.

Errata

The monthly progress reports for March and May 1984 contained the following typographical errors:

In March, the impact orientation for the SVT-6 module was 90°, not 90°C (p. 1).

In May, Table II should read Velocity (m/s), not Velocity (m/c) (p. 4).

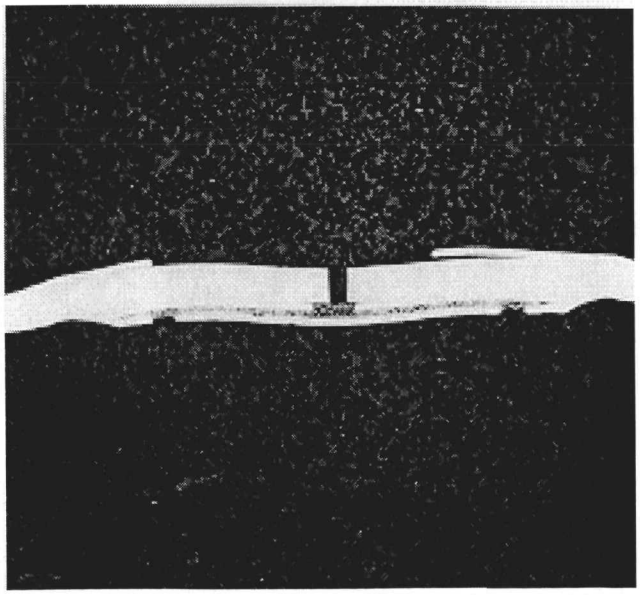

Fig. 1. No defects were observed in the vent on capsule HF-361; 7X.

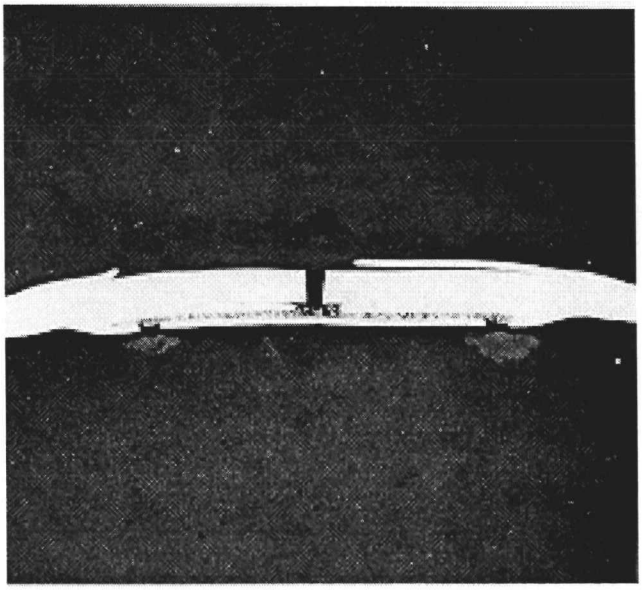

Fig. 2. The vent on capsule HF-373 was free of mechanical defects; 7X.

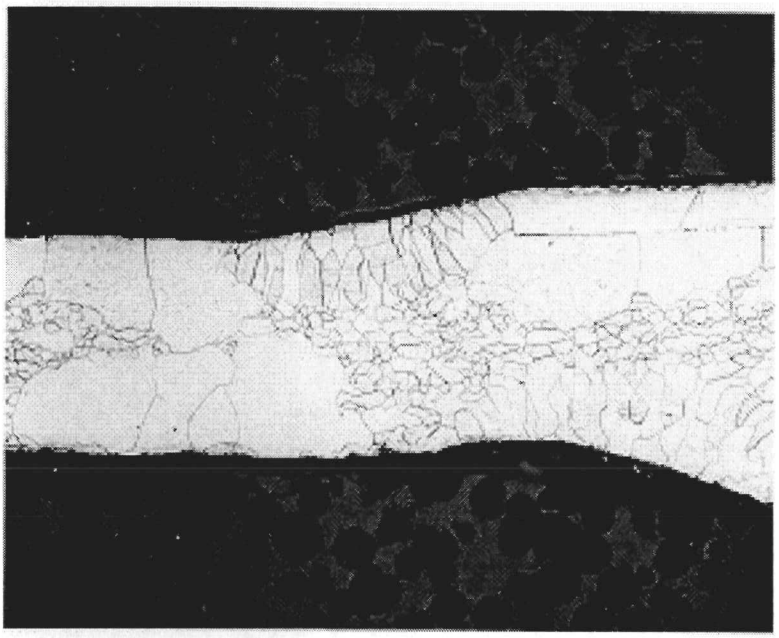

Fig. 3. An unusual amount of grain growth was observed near the cover weld on the impact-face side of the HF-361 vent section; 40X.

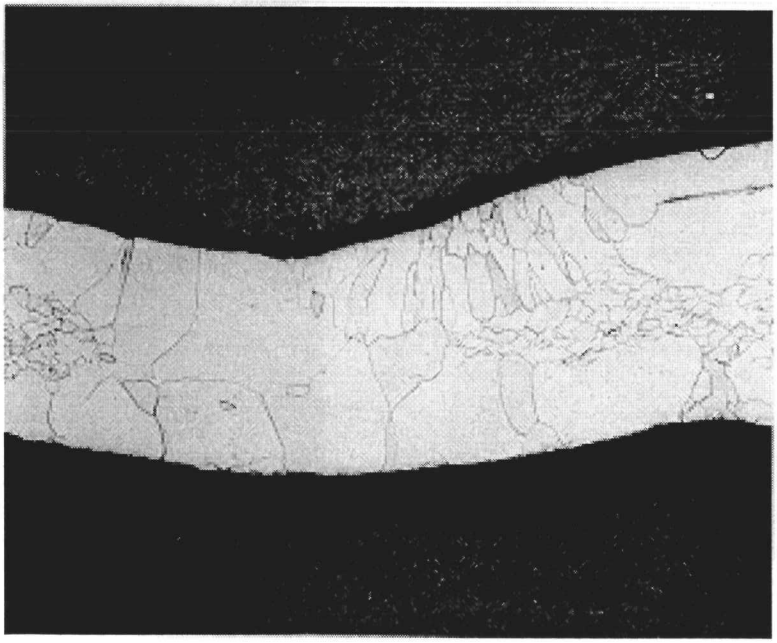

Fig. 4. Unusually large grains were observed adjacent to the vent cover and assembly welds on both sides of the HF-373 vent section; 40X.

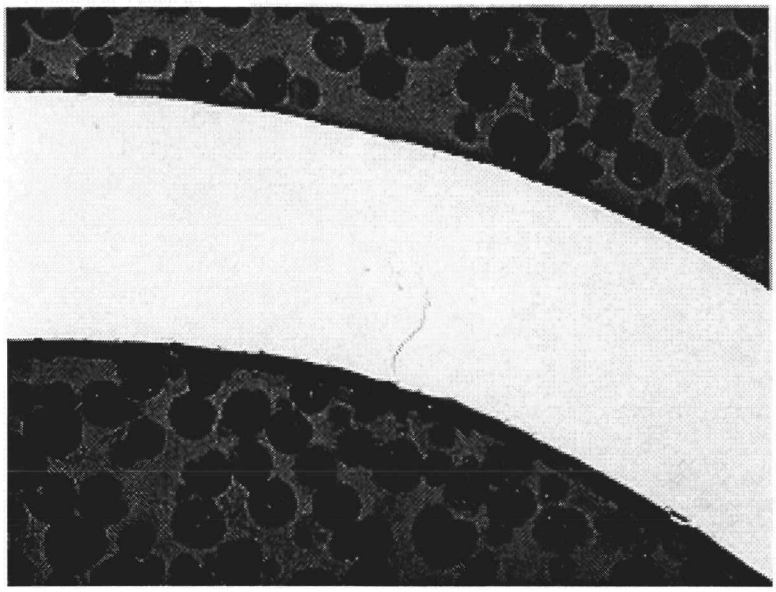

(a)

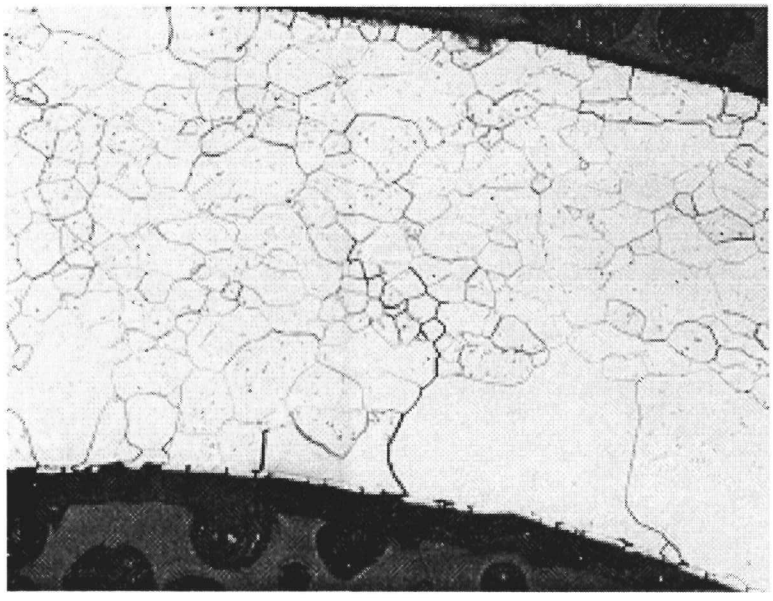

(b)

Fig. 5. Deep cracks were observed on the HF-361 vent cup radius, 180° to the impact fact; (a) unetched, 50X, and (b) etched, 100X.

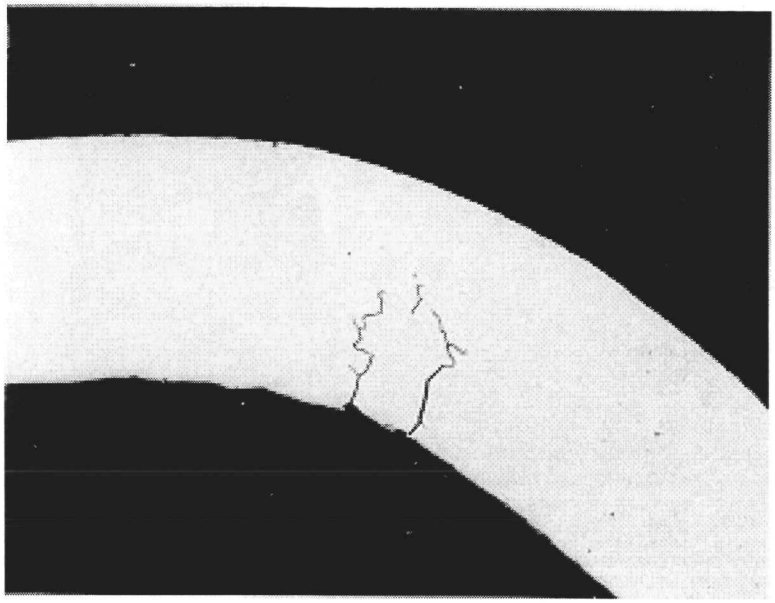

(a)

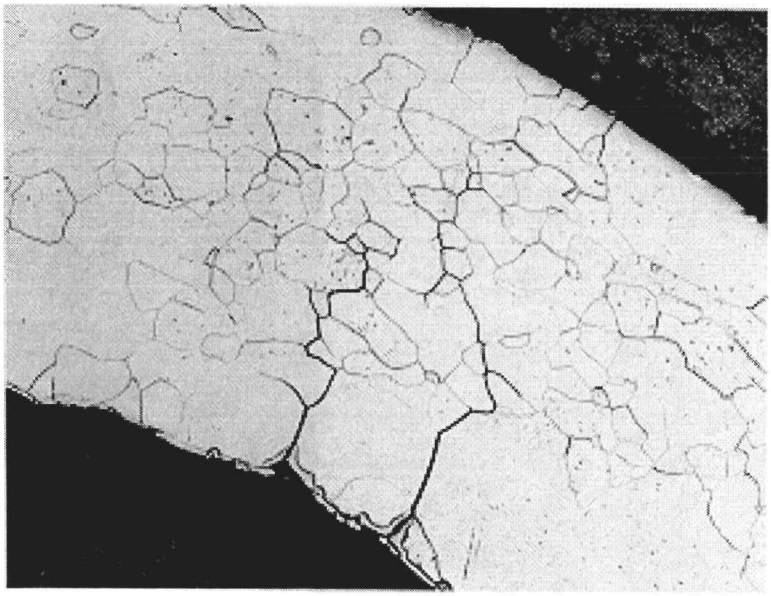

(b)

Fig. 6. Cracks on the HF-373 vent cup radius penetrated more than 65% of the wall thickness; (a) unetched, 50X, and (b) etched, 100X.

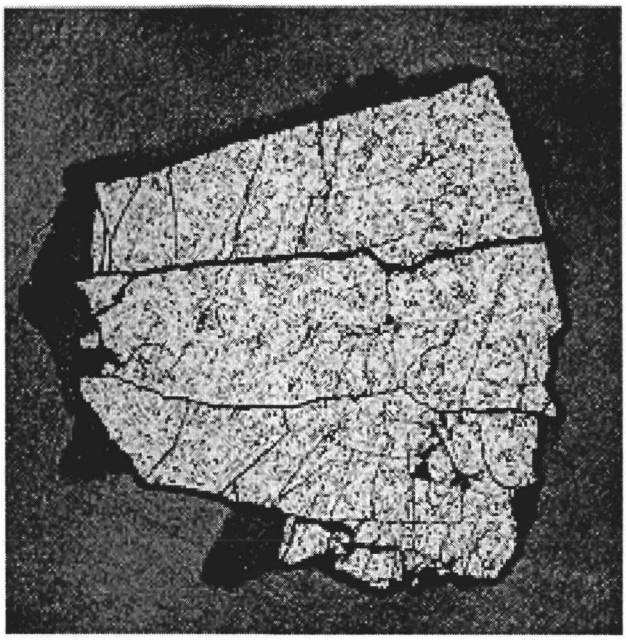

(a)

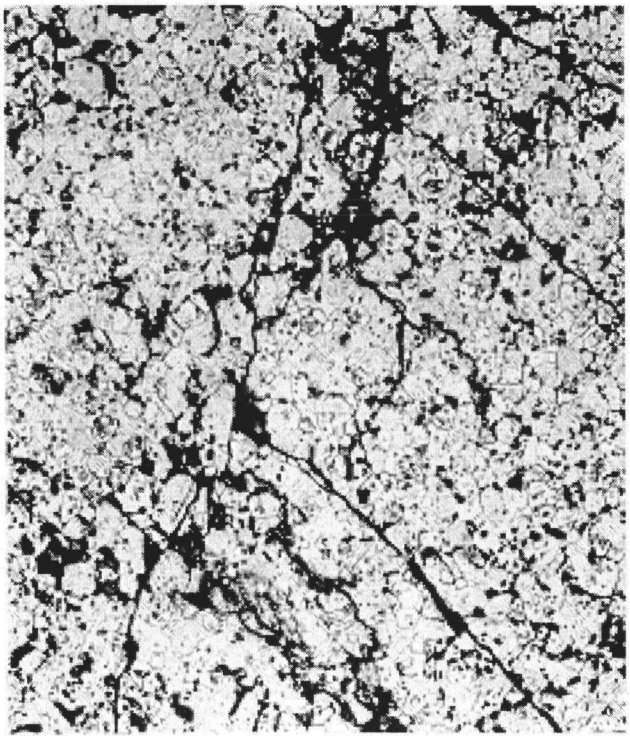

(b)

Fig. 7. The fuel in capsule HF-361 had a typical microstructure: (a) macrograph, 10X; (b) as etched, 100X.

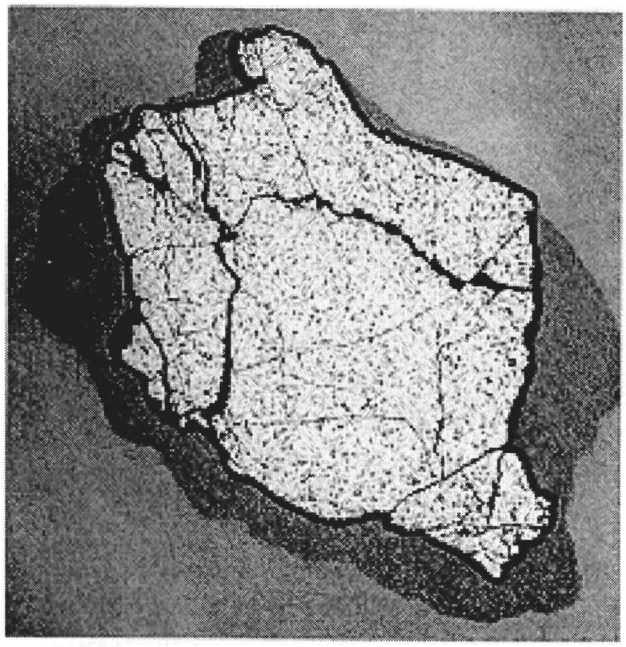

(a)

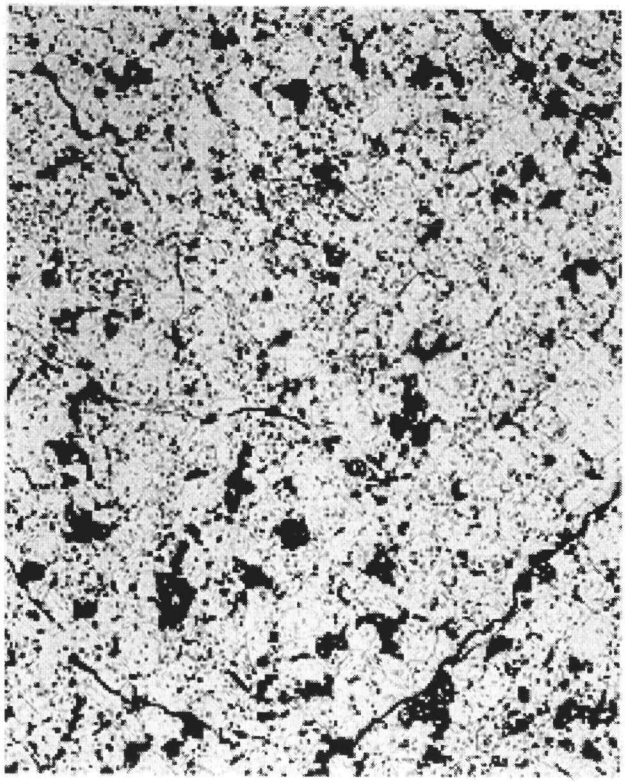

(b)

Fig. 8. The fuel in capsule HF-373 also had a typical microstructure: (a) macrograph, 10X, and (b) as etched, 100X.

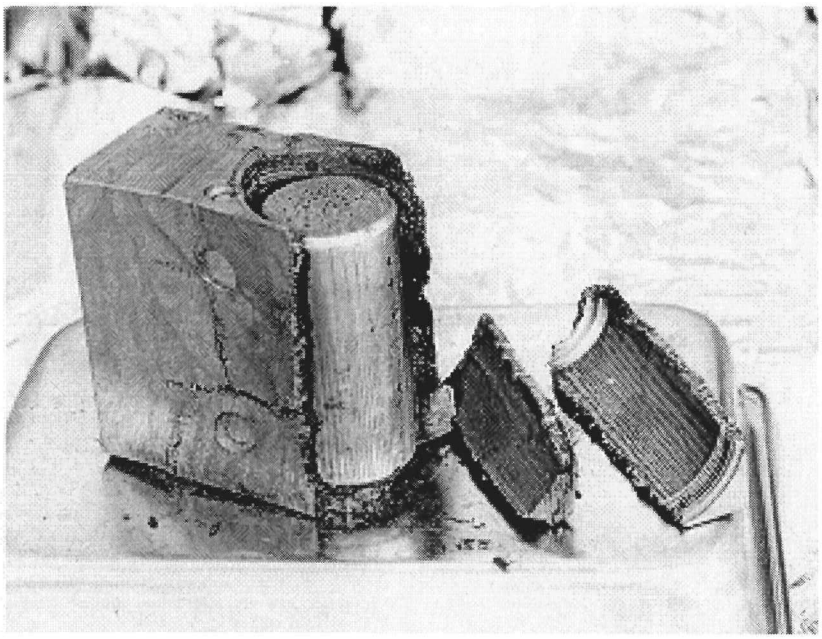

Fig. 9. Test module SVT-7 after impact. The leading narrow face of the aeroshell was separated from the body.

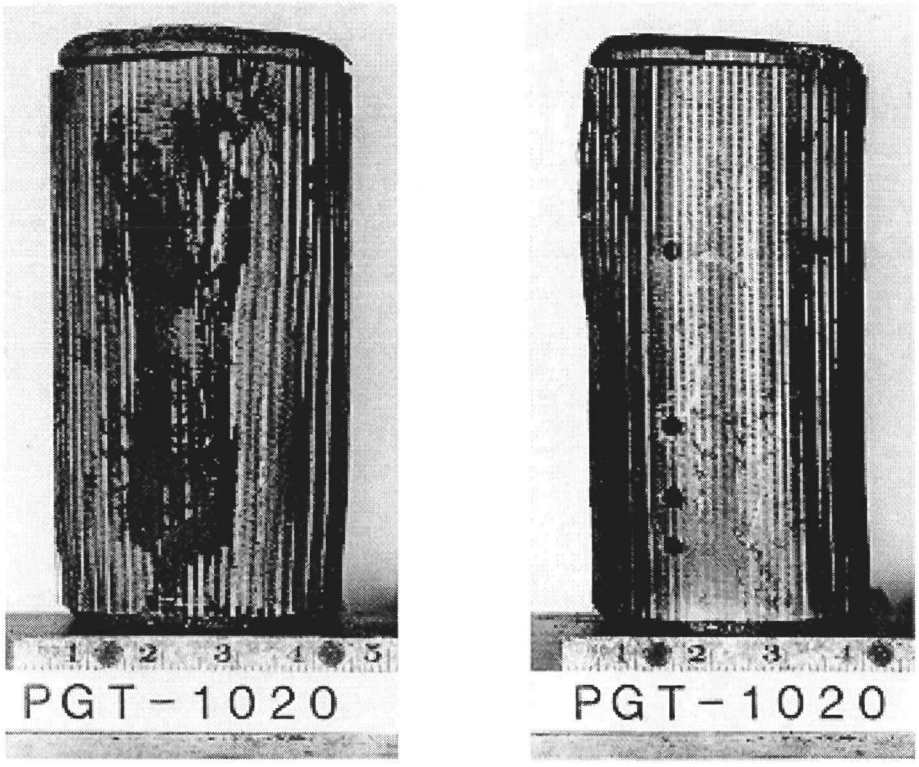

(a) (b)

Fig. 10. The leading impact assembly from SVT-7. The damage and deformation resembled that of impact tests conducted in a "face-on" orientation. (a) Impact face and (b) profile.

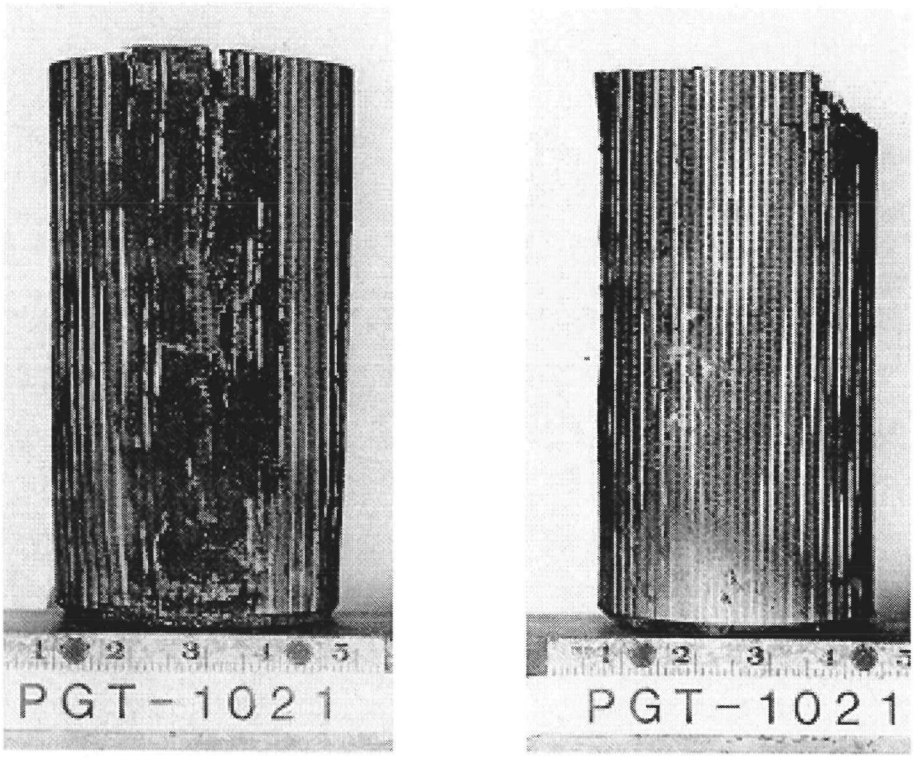

(a) (b)

Fig. 11. The trailing impact assembly from SVT-7. Damage was more severe than to the leading graphite impact shell. (a) Impact face and (b) profile view.

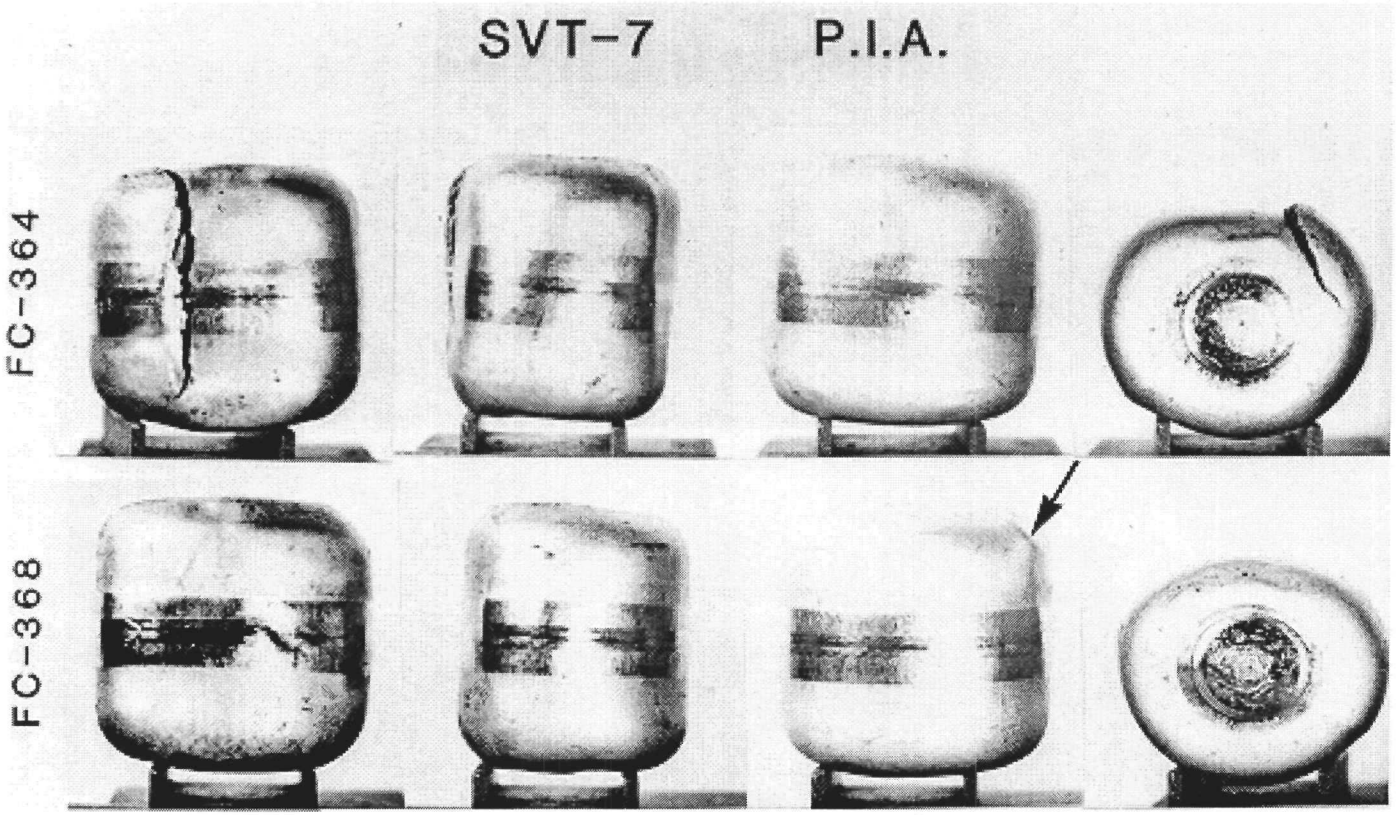

Fig. 12. The impacted fueled clads of the primary impact assembly of SVT-7. A major fuel-fragment push-through failure occurred in FC-364, and a minor fracture in FC-368 (arrow) was observed. Left to right: impact face, side profile, back side, and vent-end profile.

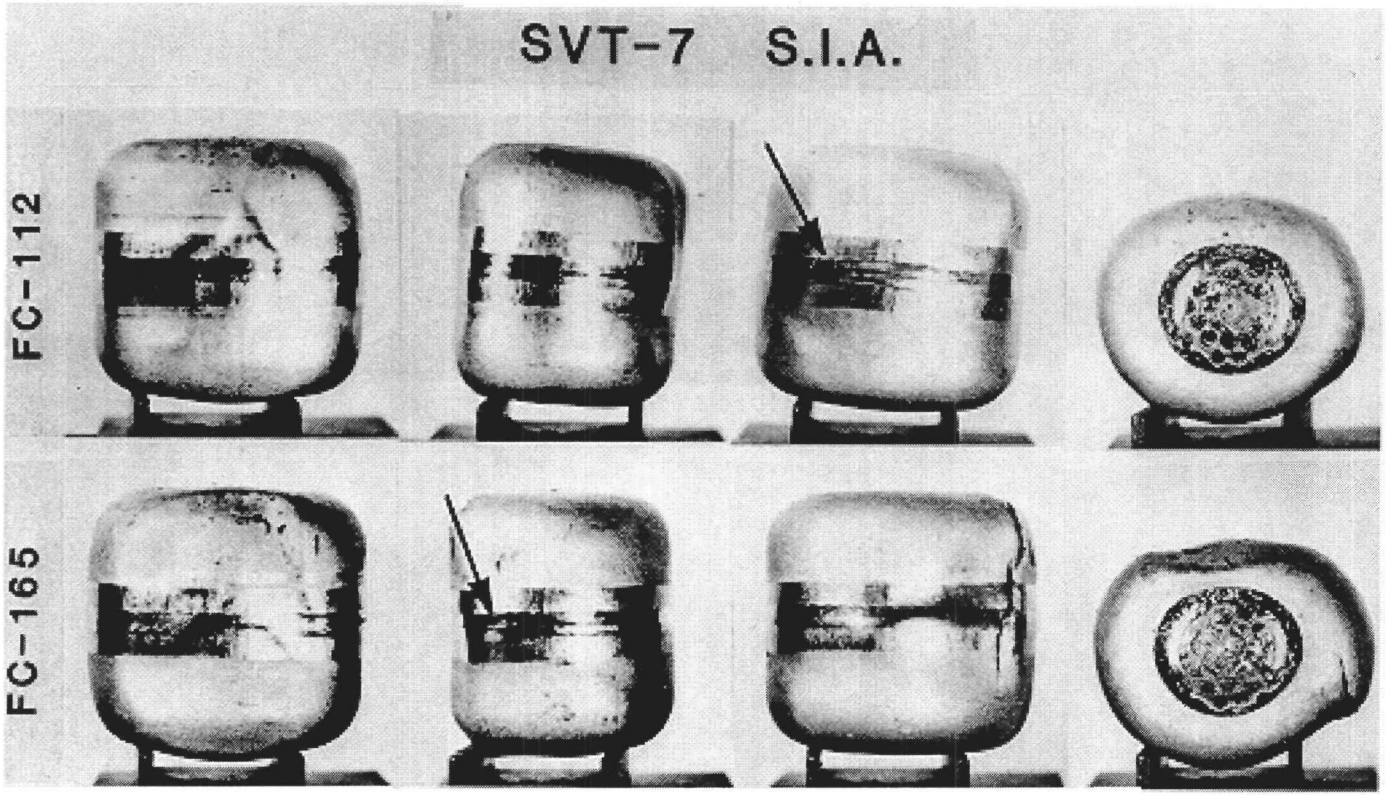

Fig. 13. The impacted fueled clads of the SVT-7 secondary impact assembly. FC-165 sustained a major fracture on the back side. Arrows indicate the location of weld-bead fractures on the back side of FC-112 and on the side of FC-165. Left to right: impact face, side profile, back side, and vent-end profile.

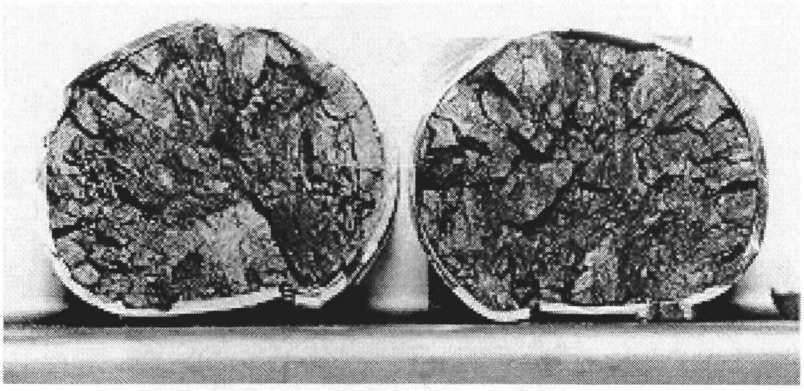

(a)

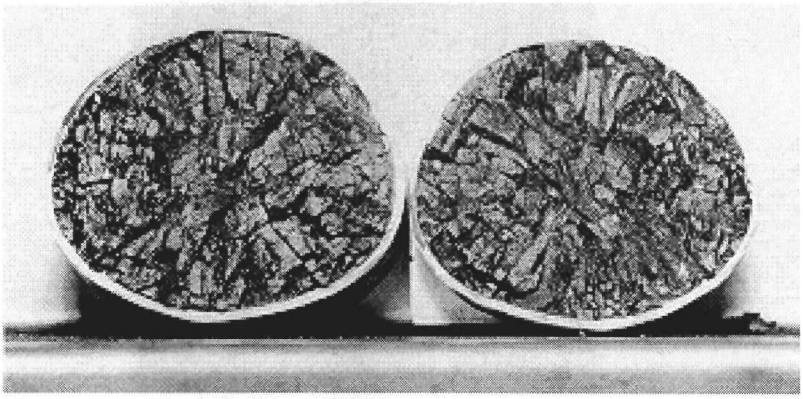

(b)

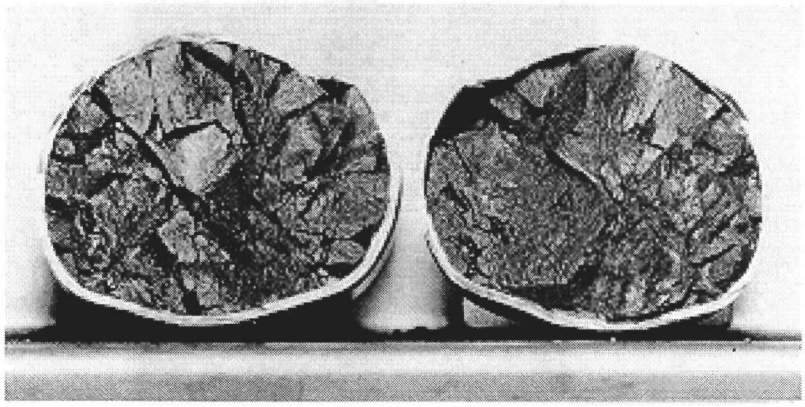

(c)

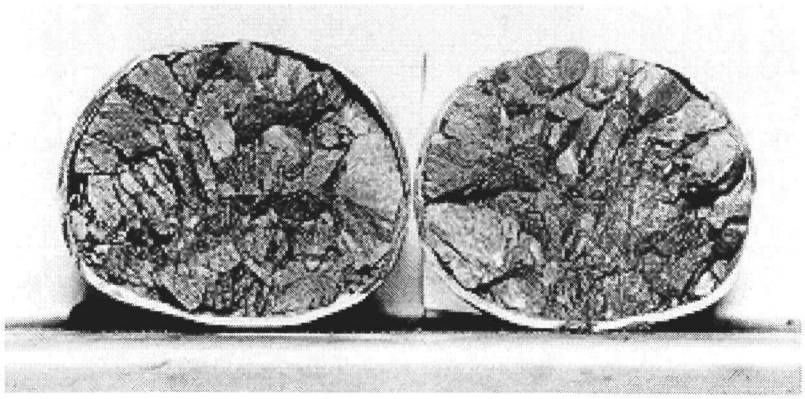

(d)

Fig. 14. The impacted plutonia pellets of SVT-7. (a) HF-364, (b) HF-368, (c) HF-165, (d) HF-112. All ~ 1.5X.

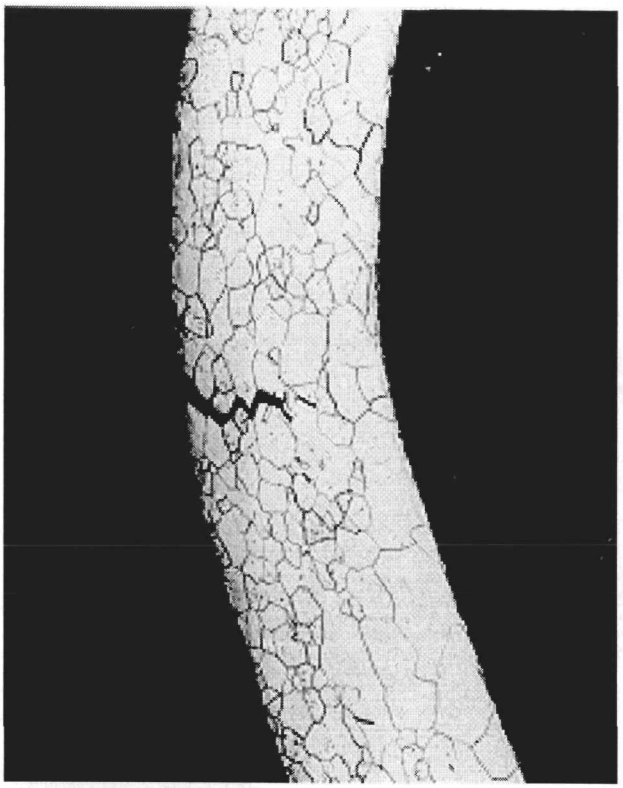

Fig. 15. Photomicrograph of the fracture in the FC-368 vent cup radius, 50X.

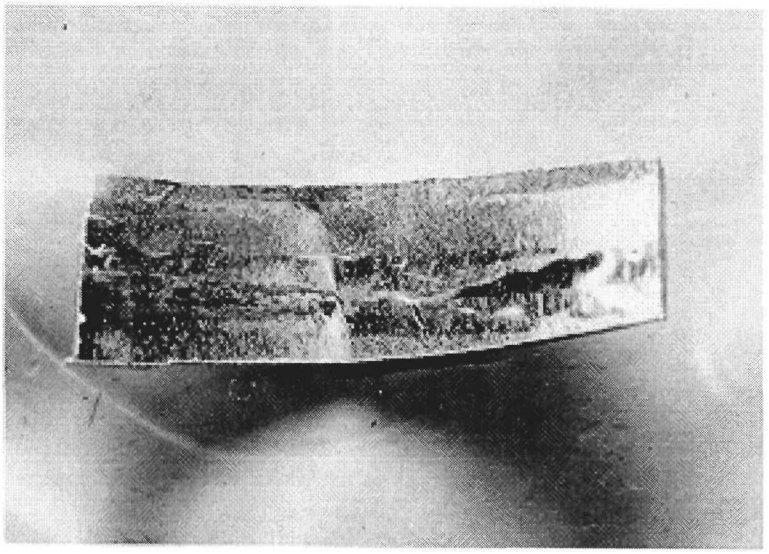

Fig. 16. The interior of the weld bead of the FC-112 clad, ~4X. The cracks occur in the vent cup side of the weld bead.

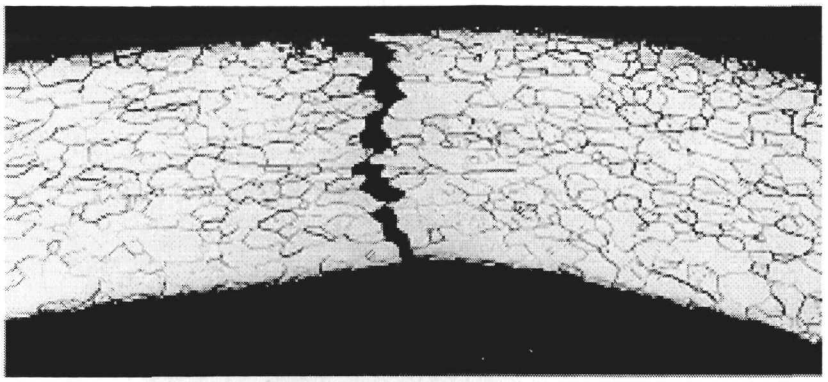

(a)

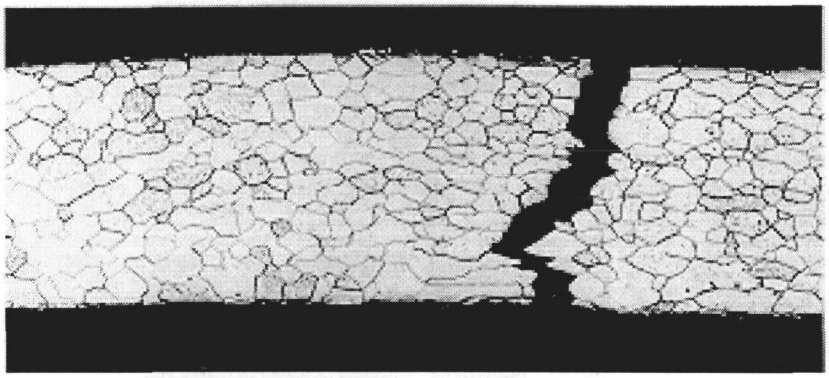

(b)

Fig. 17. Fractures in the FC-112 vent cup, above the weld; (a) and (b), 50X.

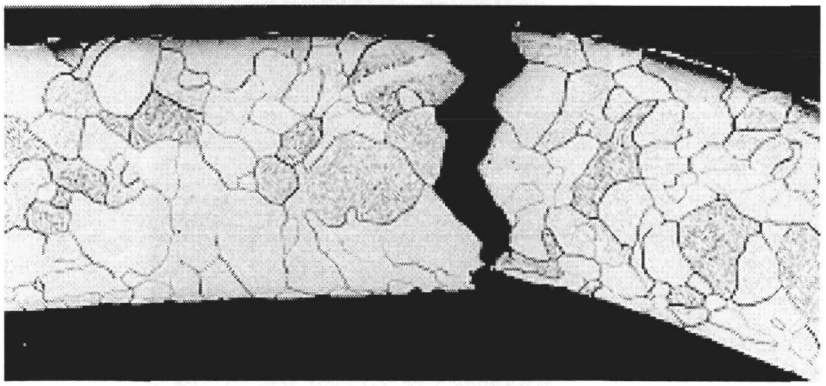

(a)

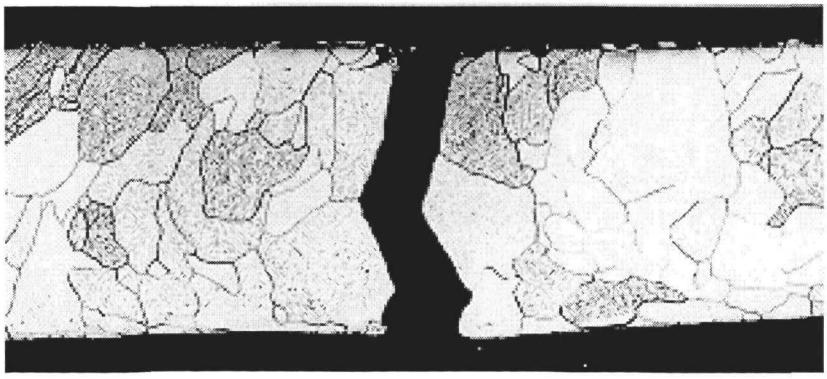

(b)

Fig. 18. The microstructure of the weld bead was relatively large grained and nearly equiaxed at the fracture sites; (a) and (b), etched, 50X.

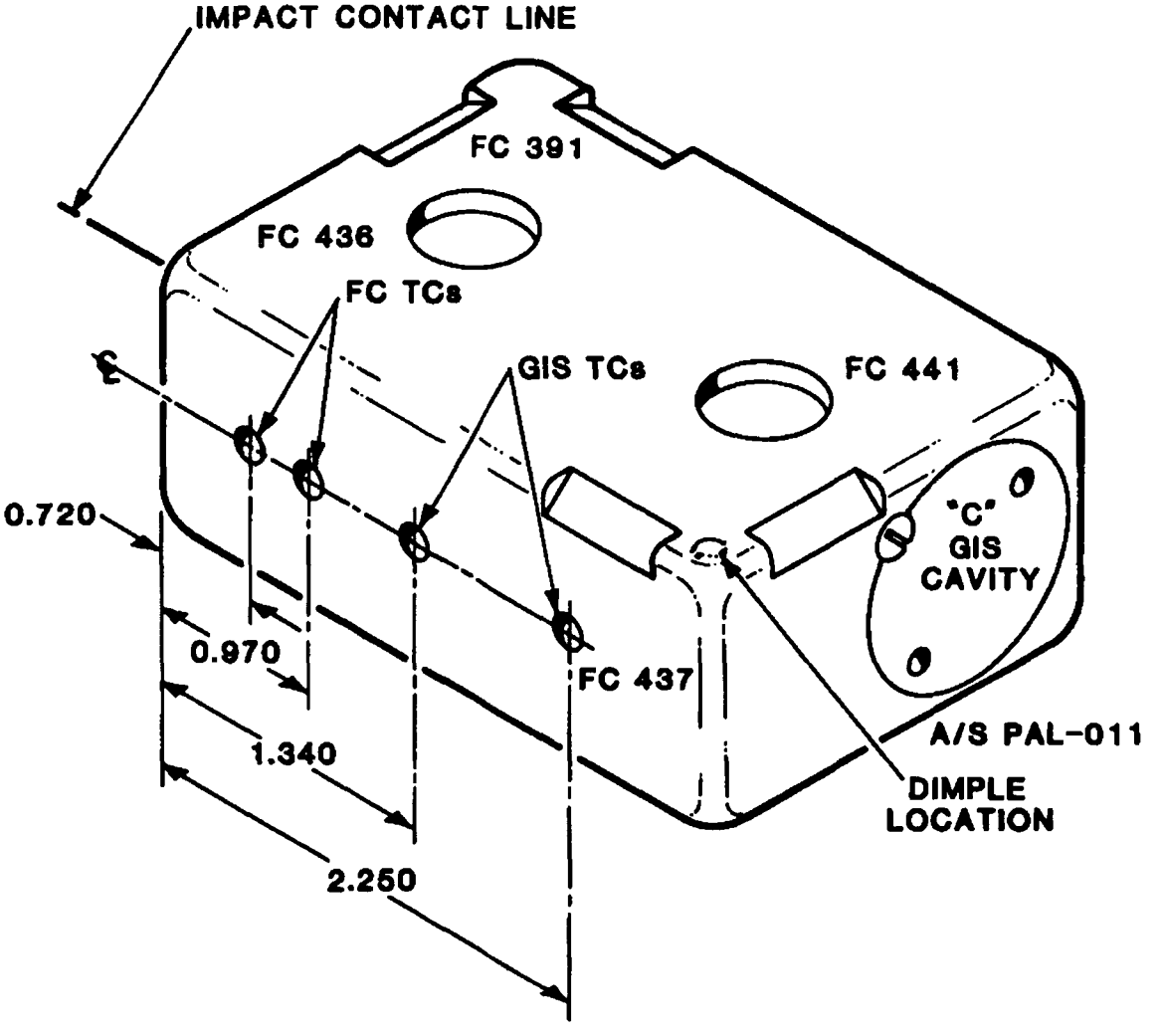

Fig. 19. SVT-8 module orientation.

Fig. 20. A large amount of debris remained in the catch tube after extraction of the SVT-8 test assembly.

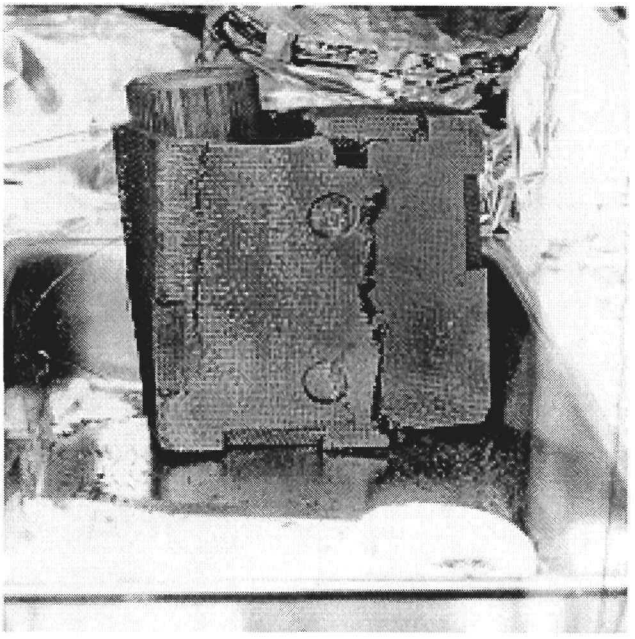

Fig. 21. The SVT-8 aeroshell fractured in several places. The impact face is on the left side of the photograph.

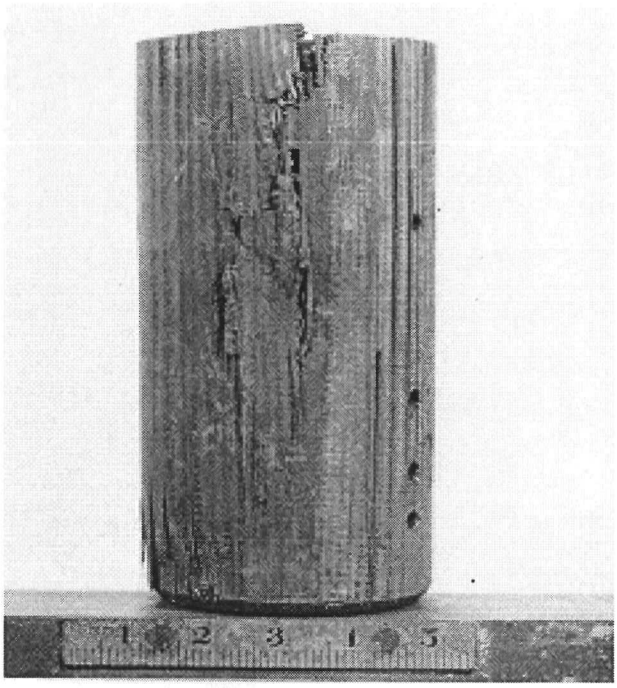

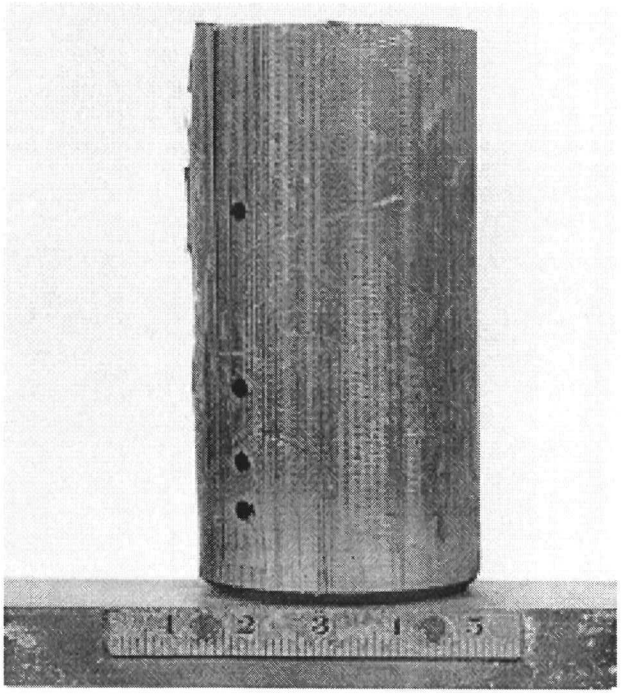

(b)

Fig. 22. Damage to the prime GIS (PGL-009) was significant but not unusual. (a) Impact face and (b) profile; both at 1X.

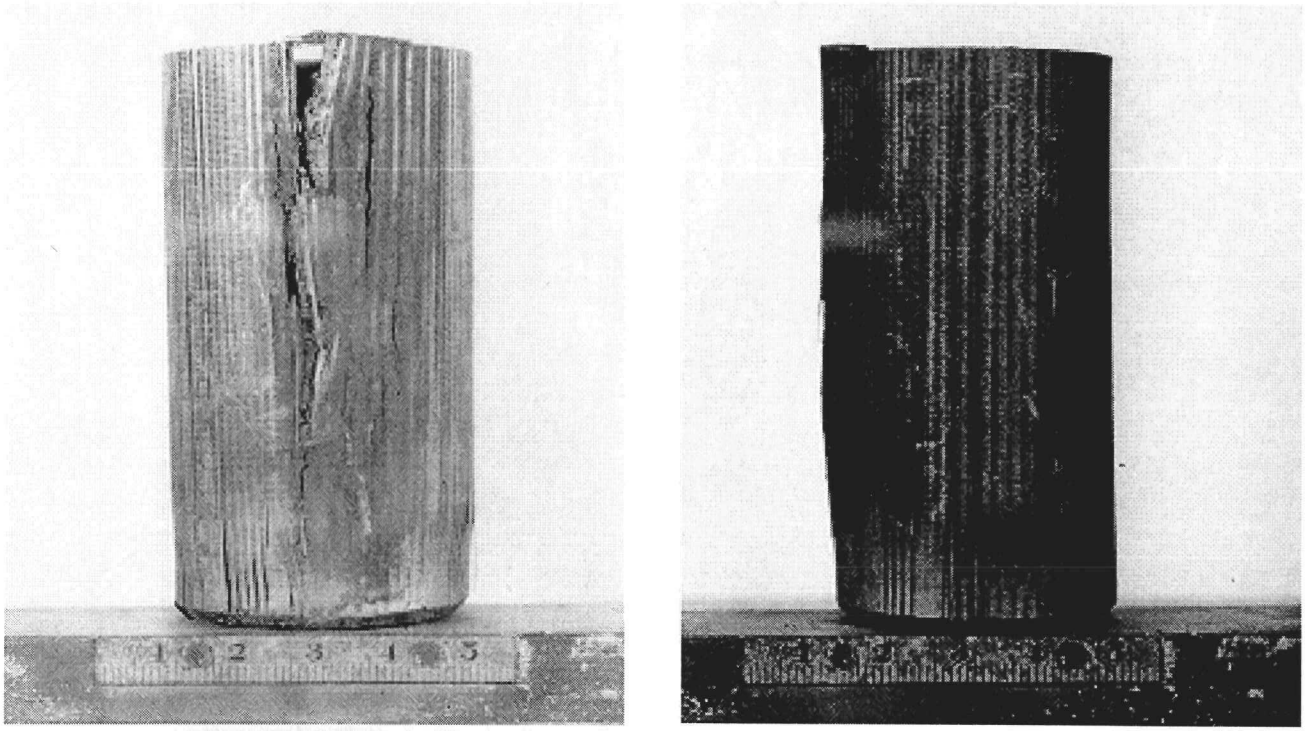

(a) (b)

Fig. 23. The trailing GIS (PGL-010) was extensively fractured on the impact face. (a) Impact face and (b) profile; both at 1X.

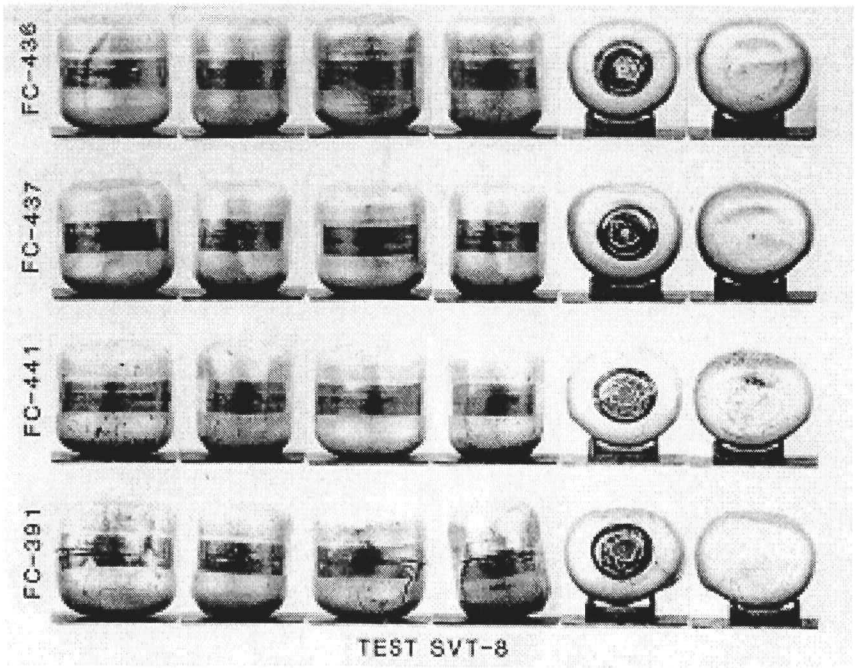

Fig. 24. The SVT-8 clads were only moderately deformed.

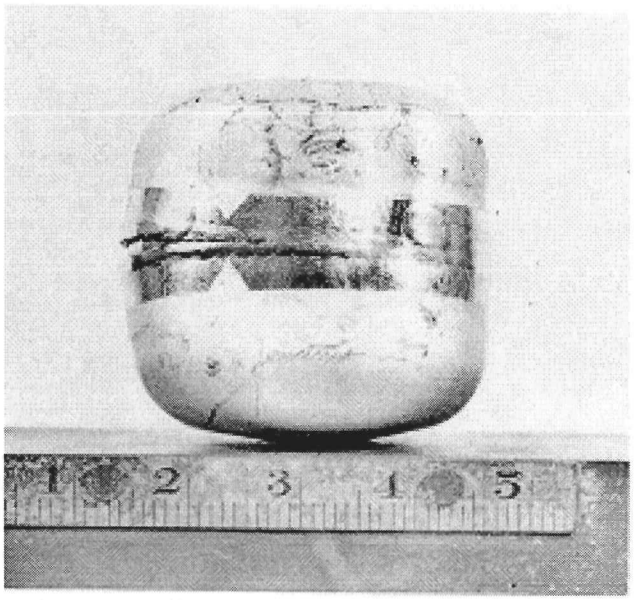

(a)

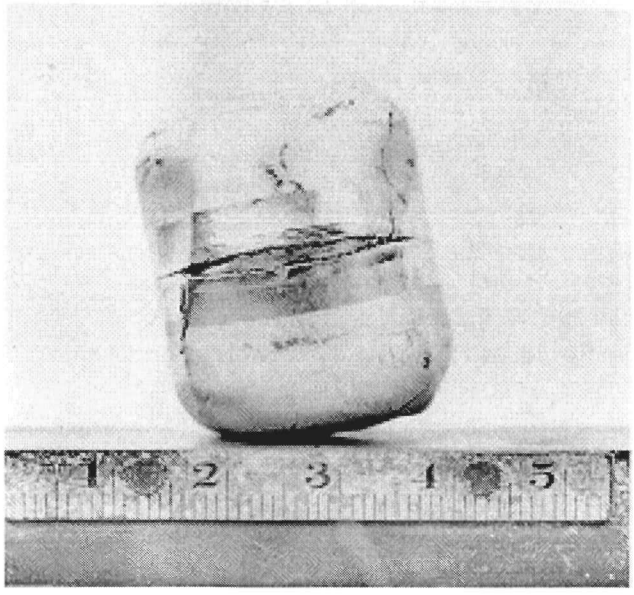

(b)

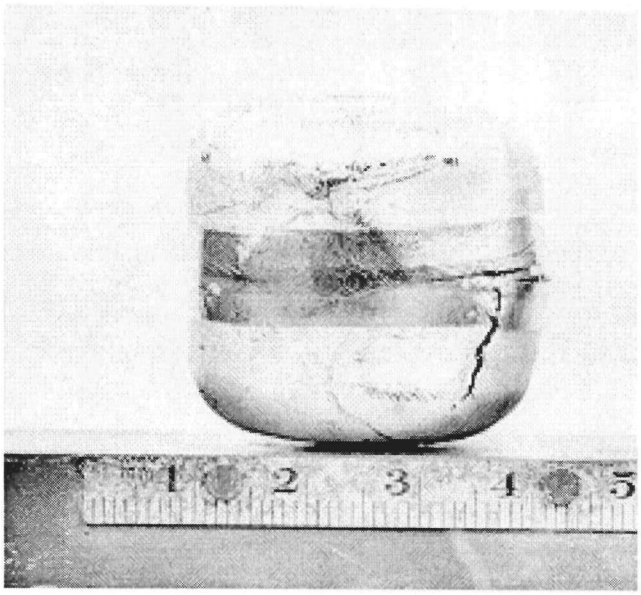

(c)

Fig. 25. The closure weld on capsule FC-391 opened over a 120° arc. (a) Impact face, (b) turned 180°, and (c) turned 270°; all at 1.5X.

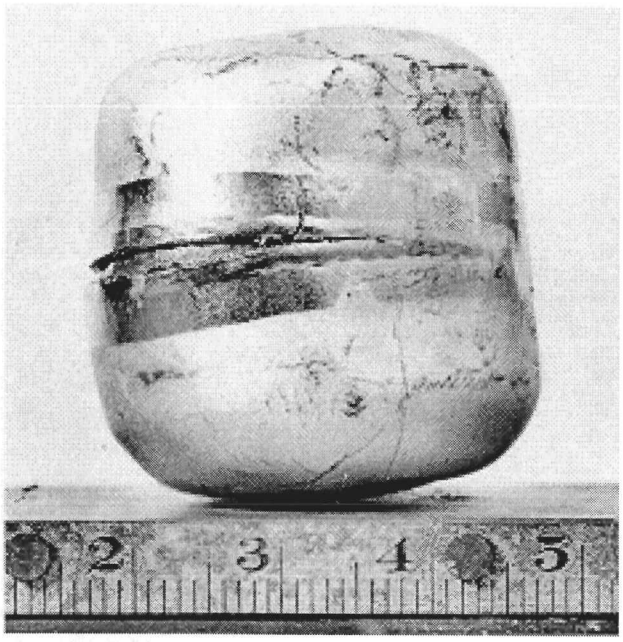

(a)

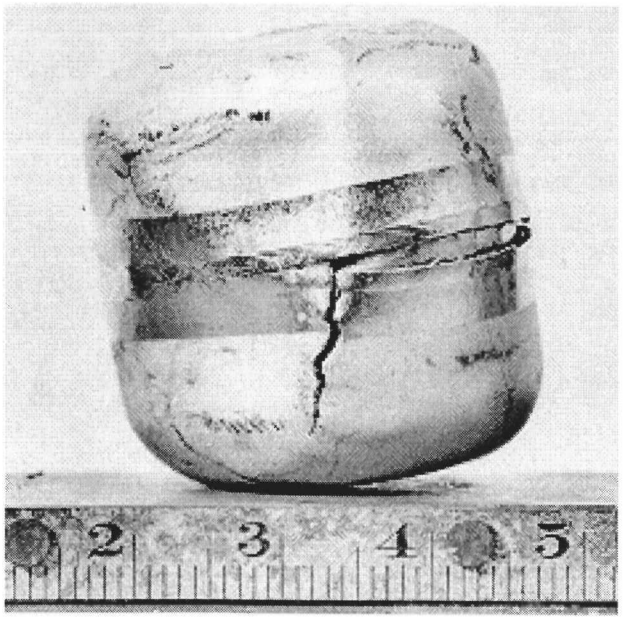

(b)

Fig. 26. The width of the main crack generated secondary cracks in the vent and weld-shield cups. (a) Impact face and (b) tearing face; both at 2X.

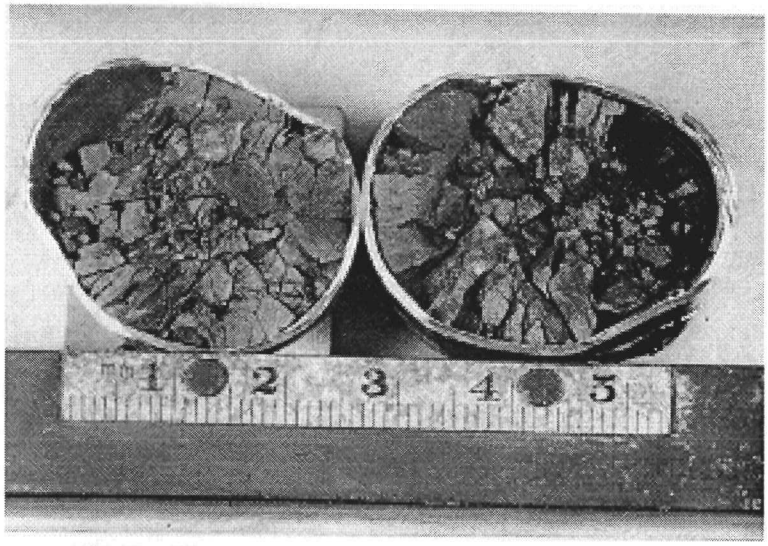

Fig. 27. The fuel in capsule FC-391 was broken into gravel-sized fragments; 1.5X.

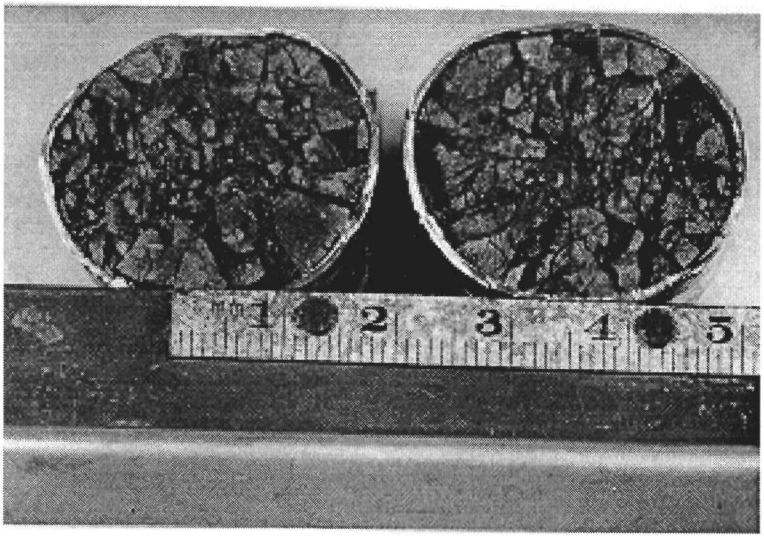

Fig. 28. The fuel in capsule FC-436 fractured into pea-sized fragments; 1.5X.

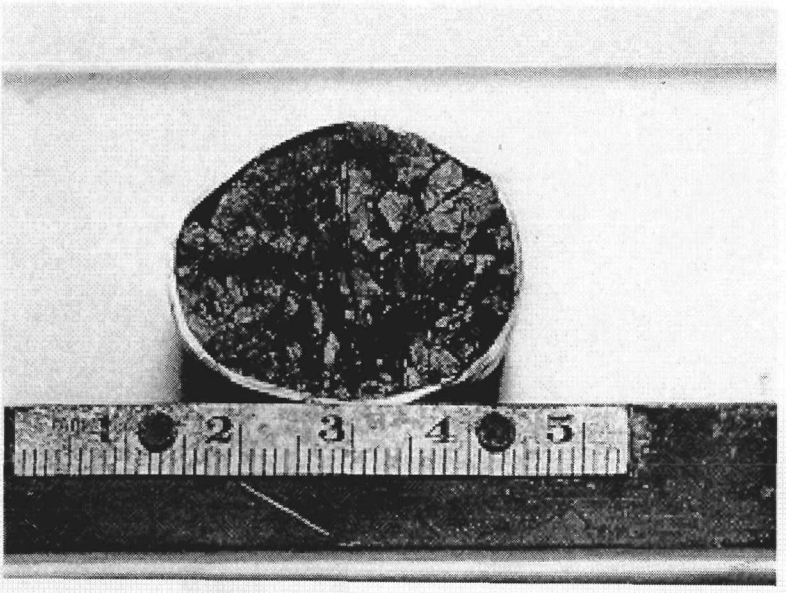

Fig. 29. The fuel in capsule FC-441 fractured in much the same manner as the fuel in capsules FC-391 and FC-436; 1.5X.

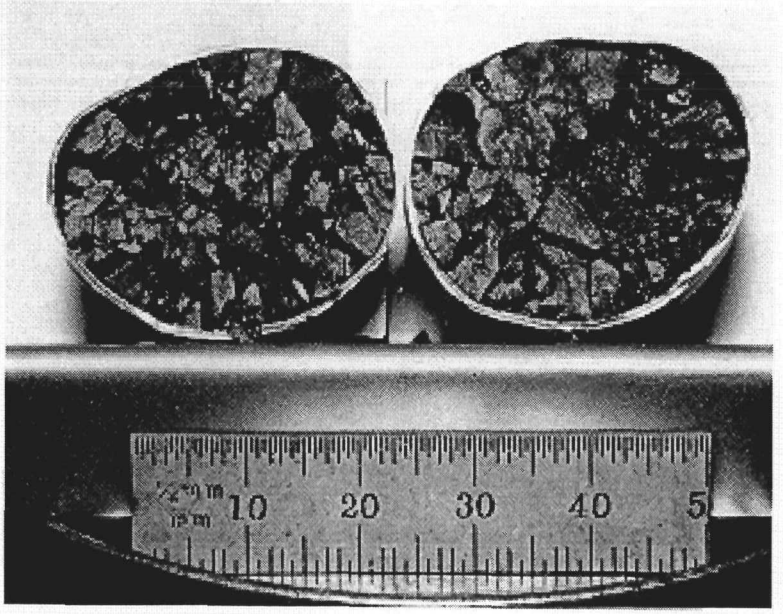

Fig. 30. The pattern of fuel breakup in capsule FC-437 was similar to that observed in the other capsules; 1.5X.

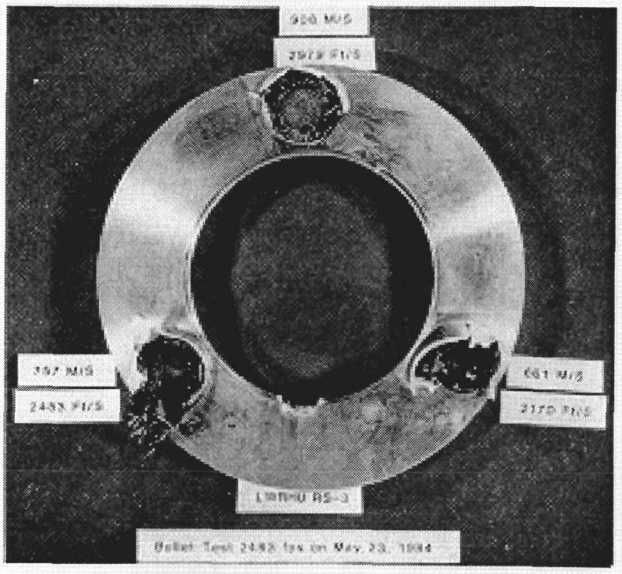

Fig. 31. Fixture for holding LWRHU capsules in bullet tests.

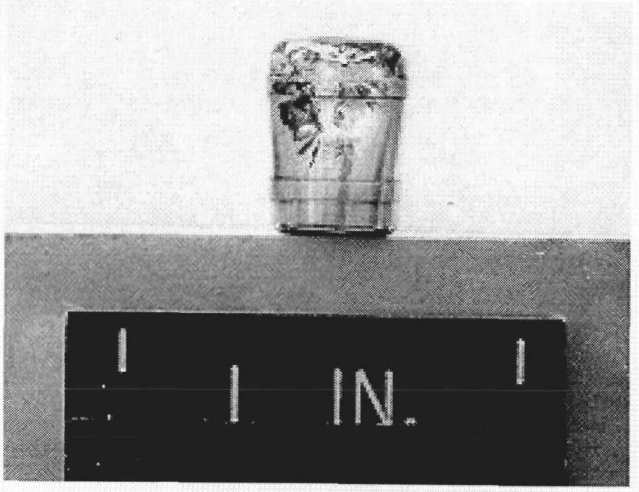

Fig. 32. Impact face of RS-3 after bullet impact at 908 m/s (2979 ft/s), ~2X.

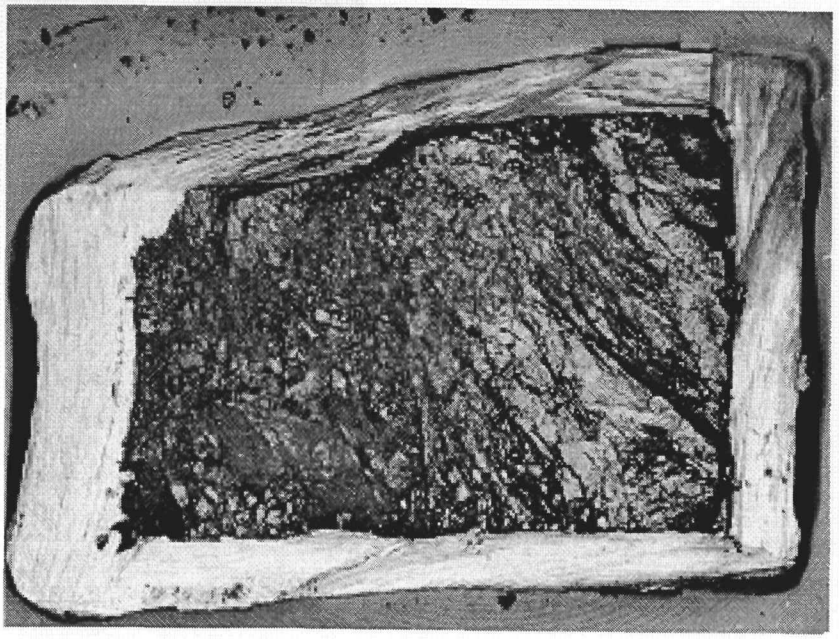

Fig. 33. Longitudinal section of RS-3 with fuel intact, ~8X.

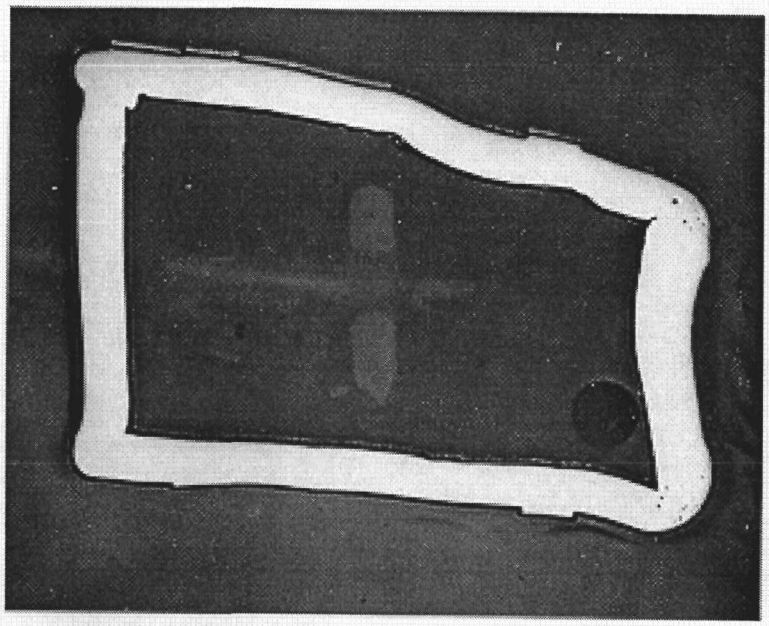

(a)

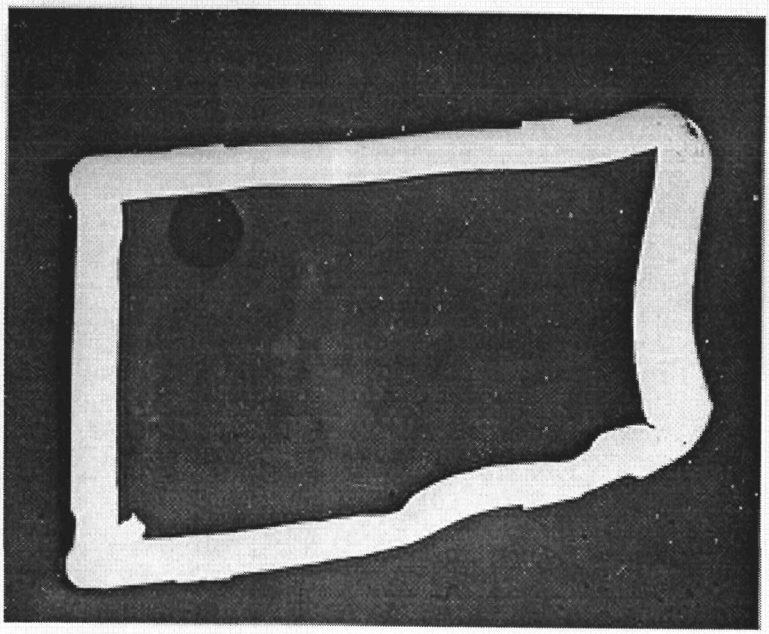

(b)

Fig. 34. Longitudinal sections of RS-3, (a) and (b) as polished. ~7X.

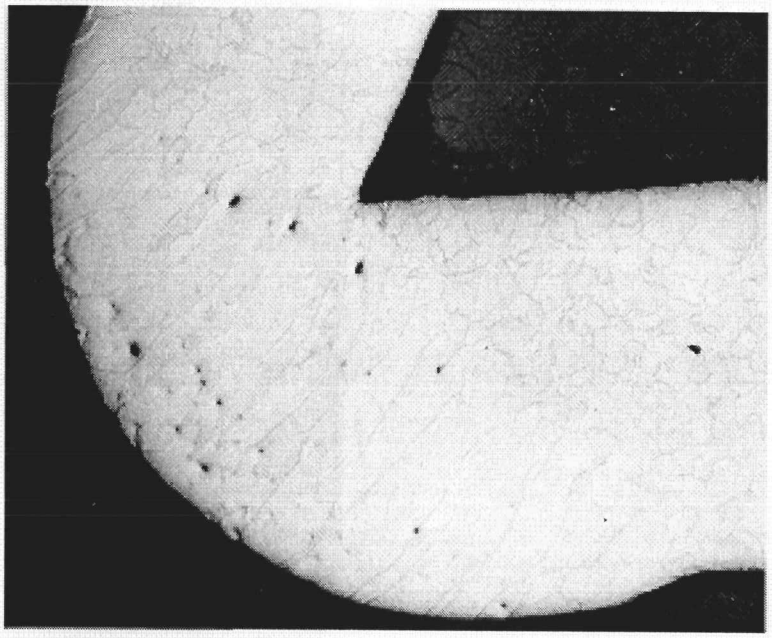

Fig. 35. Closure weld section of RS-3, as etched, 50X.

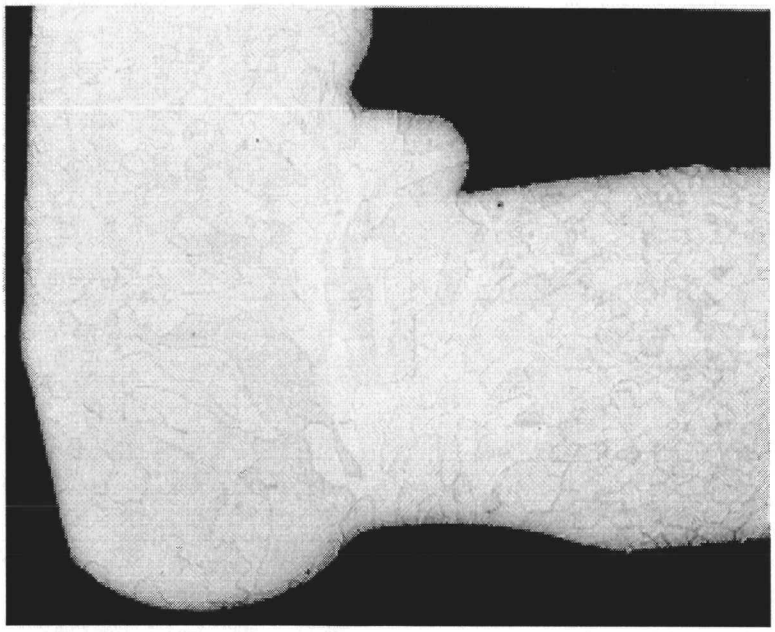

(a)

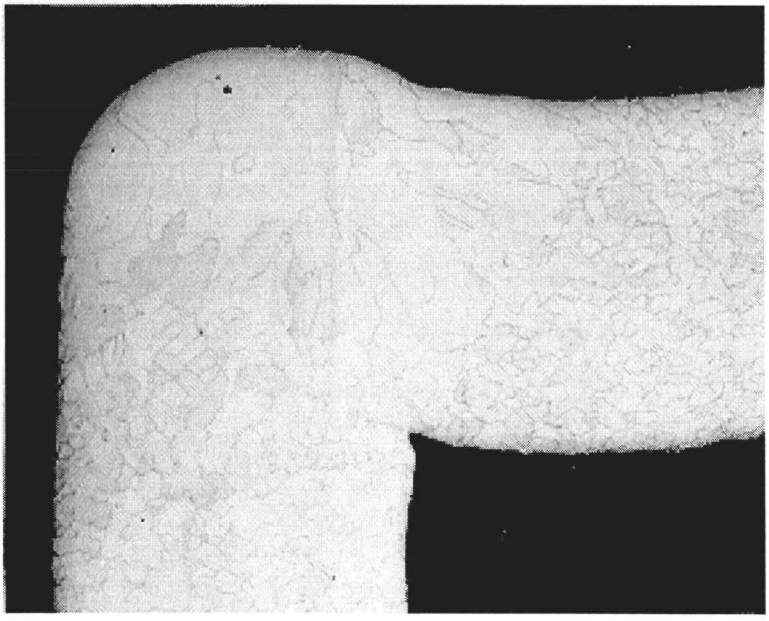

(b)

Fig. 36. The RS-3 vent-end weld was somewhat heavy but acceptable. Opposite corners, (a) and (b), as etched, 50X.

ADDITIONAL DISTRIBUTION

B. J. Rock, Dept. of Energy/OSNP, Washington, DC
G. L. Bennett, Dept. of Energy/OSNP, Washington, DC
J. J. Lombardo, Dept. of Energy/OSNP, Washington, DC
R. B. Morrow, Dept. of Energy/OSNP, Washington, DC
R. Brouns, Dept. of Energy/OSNP, Washington, DC
J. Griffo, Dept. of Energy/OSNP, Washington, DC
D. K. Stevens, Dept. of Energy/BES, Washington, DC
M. Norin, Dept. of Energy, Washington, DC
N. P. Klug, Dept. of Energy, Washington, DC
L. Smith, Dept. of Energy, Washington, DC
E. Bjoro, Dept. of Energy, Washington, DC
G. H. Ogburn, Dept. of Energy, Washington, DC
J. A. Yoder, Dept. of Energy, Washington, DC
C. Osterberg, Dept. of Energy, Washington, DC
I. Van Der Hoven, Dept. of Energy, Rockville, MD
J. V. Dorigan, Dept. of Energy, Washington, DC
W. O. Forster, Dept. of Energy, Washington, DC
R. Watters, Dept. of Energy, Washington, DC
H. B. Rosenthal, Dept. of Energy, Washington, DC
Col. Terry Hawkins, ATSD (AE), Dept. of Defense, Washington, DC
Lt. Col. Jim Greening, HQ USAF/IG, Dept. of Defense, Washington, DC
D. L. Foster, Dept. of Energy, Albuquerque, NM
J. P. Crane, Dept. of Energy, Albuquerque, NM
K. Elliot, Dept. of Energy, Albuquerque, NM
D. L. Krenz, Dept. of Energy, Albuquerque, NM
J. R. Roeder, Dept. of Energy, Albuquerque, NM
R. B. Crouch, Dept. of Energy, Albuquerque, NM
J. N. Bailey, Dept. of Energy, Albuquerque, NM
H. N. Hill, Dept. of Energy/DOA, Miamisburg, OH
L. C. Sjostrom, Dept. of Energy, Aiken, SC
S. W. Ahrends, Dept. of Energy/ORO, Oak Ridge, TN
R. J. Hart, Dept. of Energy/ORO, Oak Ridge, TN
J. Pidkowicz, Dept. of Energy, Oak Ridge, TN
W. L. Von Flue, Dept. of Energy, SFOO, Oakland, CA
T. B. Kerr, NASA, Washington, DC
F. R. Schmidt, NASA, Washington, DC
E. Gabris, NASA, Washington, DC
N. Sculze, NASA, Washington, DC
B. R. McCullar, NASA, Washington, DC
Operations Space Shuttle, NASA, Washington, DC
A. V. Diaz, NASA, Washington, DC
R. G. Ivanoff, Jet Propulsion Laboratory, Pasadena, CA
R. W. Campbell, Jet Propulsion Laboratory, Pasadena, CA
L. C. Montgomery, Jet Propulsion Laboratory, Pasadena, CA
L. T. Shaw, Jet Propulsion Laboratory, Pasadena, CA
R. J. Spehalski, Jet Propulsion Laboratory, Pasadena, CA
Dr. Agnus D. McRonald, Jet Propulsion Laboratory, Pasadena, CA
P. Jaffe, Jet Propulsion Laboratory, Pasadena, CA
AFWL/SNS, Attn: Col. J. A. Richardson, Kirtland AFB, NM
AFWL/NTYNS, Attn: Capt. D. E. Zimmerman, Kirtland AFB, NM
Lt. Col. James H. Lee, Jr., AFWL/NTYN, Kirtland AFB, NM
Capt. Michael K. Seaton, AFWL/NTYNP, Kirtland AFB, NM
Col. John Joyce, AFISC/SND, Kirtland, AFB, NM
Maj. John Rice, AFISC/SNA, Kirtland AFB, NM
P. Dick, Teledyne Energy Systems, Timonium, MD
M. Goldman, University of California, Davis, CA
C. Smith, Sandia National Laboratories, Albuquerque, NM
R. L. Hannigan, Sandia National Laboratories, Albuquerque, NM
R. Harner, Sandia National Laboratories, Albuquerque, NM
C. M. Barnes, L. B. Johnson Space Center, NASA, Houston, TX
R. H. Brown, L. B. Johnson Space Center, NASA FM, Houston, TX
R. G. Rose, L. B. Johnson Space Center, NASA FA, Houston, TX
Harold Battaglia, L. B. Johnson Space Center, NASA PF, Houston, TX
W. H. Boggs, NASA, DE-A, J. F. Kennedy Space Center, FL
Lloyd Parker, NASA, SF, J. F. Kennedy Space Center, FL
George M. Marmaro, NASA, MD-ENV, J. F. Kennedy Space Center, FL
W. A. Riehl, Marshall Space Flight Center, NASA, EH31, Marshall SFC, AL
W. C. Pitts, NASA, STPM, Ames Research Center, Moffett Field, CA
J. J. Givens, Ames Research Center, Moffett Field, CA
R. Corridan, Ames Research Center-NASA, Moffett Field, CA
Kenneth Sutton, Langley Research Center, NASA, Hampton, VA
Gerald D. Walberg, Langley Research Center, NASA, Hampton, VA
G. J. Schaefer, Jr., Lewis Research Center, NASA, LeRc-501, Cleveland, OH
R. C. Turkolu, TRW, Defense and Space Systems Group, Redondo Beach, CA
D. Eaton, European Space Research and Technology Centre, Zwarteweg 62, Njordwijk, The Netherlands
Dr. Ralph R. Fullwood, Science Applications, Inc., Palo Alto, CA
D. Glenn, The Aerospace Corporation, Los Angeles, CA
Dr. William Ailor, The Aerospace Corporation, Los Angeles, CA
T. Carter, Nuclear Regulatory Commission, Washington, DC
C. R. Chappell, Nuclear Regulatory Commission, Washington, DC
D. E. Janes, U. S. Environmental Protection Agency, Washington, DC
D. Eagan, Office of Radiation Programs, Washington, DC
James Boland, Argonne National Laboratory-West, Idaho Falls, ID
N. Elsner, General Atomics, San Diego, CA
R. F. Abbey, Naval Research Laboratory, Washington, DC
Charles Salisbury, Naval Ocean Systems Center, San Diego, CA
Dr. Herbert Weiss, Naval Ocean Systems Center, San Diego, CA
R. Cuddihy, IIT Research Institute, Chicago, IL
J. F. Park, Pacific Northwest Laboratory, Richland, WA
Thomas M. Beasley, Oregon State University, Newport, OR
Jackson O. Blanton, Skidaway Inst. of Oceanography, Savannah, GA
Martha Scott, Texas A&M University, College Station, TX
H. James Simpson, Columbia University, Palisades, NY
S. S. Hecker, Los Alamos National Laboratory, Los Alamos, NM
R. N. R. Mulford, Los Alamos National Laboratory, Los Alamos, NM
J. Birely, Los Alamos National Laboratory, Los Alamos, NM
S. E. Bronisz, Los Alamos National Laboratory, Los Alamos, NM
W. Stark, Los Alamos National Laboratory, Los Alamos, NM
R. W. Zocher, Los Alamos National Laboratory, Los Alamos, NM
J. A. Pattillo, Los Alamos National Laboratory, Los Alamos, NM
E. M. Wewerka, Los Alamos National Laboratory, Los Alamos, NM
T. C. Wallace, Los Alamos National Laboratory, Los Alamos, NM
T. K. Keenan, Los Alamos National Laboratory, Los Alamos, NM
C. M. Seabourn, Los Alamos National Laboratory, Los Alamos, NM
P. Wagner, Los Alamos National Laboratory, Los Alamos, NM

☆ U S Government Printing Office 1985-676-104/20014